Anniversary Paper: Evolution of ultrasound physics and the role of medical physicists and the AAPM and its journal in that evolution

Paul L. Carson[a)]
Basic Radiological Sciences Collegiate Professor, Department of Radiology, University of Michigan Health System, 3218C Medical Science I, B Wing SPC 5667, 1301 Catherine Street, Ann Arbor, Michigan 48109-5667

Aaron Fenster
Imaging Research Laboratories, Robarts Research Institute, 100 Perth Drive, P. O. Box 5015, London, Ontario N6A 5K8, Canada

(Received 26 May 2008; revised 8 September 2008; accepted for publication 9 September 2008; published 13 January 2009)

Ultrasound has been the greatest imaging modality worldwide for many years by equipment purchase value and by number of machines and examinations. It is becoming increasingly the front end imaging modality; serving often as an extension of the physician's fingers. We believe that at the other extreme, high-end systems will continue to compete with all other imaging modalities in imaging departments to be the method of choice for various applications, particularly where safety and cost are paramount. Therapeutic ultrasound, in addition to the physiotherapy practiced for many decades, is just coming into its own as a major tool in the long progression to less invasive interventional treatment. The physics of medical ultrasound has evolved over many fronts throughout its history. For this reason, a topical review, rather than a primarily chronological one is presented. A brief review of medical ultrasound imaging and therapy is presented, with an emphasis on the contributions of medical physicists, the American Association of Physicists in Medicine (AAPM) and its publications, particularly its journal *Medical Physics*. The AAPM and Medical Physics have contributed substantially to training of physicists and engineers, medical practitioners, technologists, and the public.
[DOI: 10.1118/1.2992048]

I. INTRODUCTION

Ultrasound imaging was the first effective soft tissue imaging modality used in diagnostic radiology as it provided tomographic views of the anatomy. After the introduction of ultrasound imaging, computed tomography (CT) and Magnetic Resonance Imaging (MRI) were introduced for disease diagnosis and management. Although CT and MRI are used extensively, ultrasound imaging provides unique advantages over CT and MRI with its ability for real-time imaging, its low cost, and small size allowing imaging at the patient's bedside. Ultrasound imaging and therapy, as a major imaging and a promising treatment modality, have drawn the attention of numerous medical physicists and medical physics groups. A good model for ultrasound in medical physics programs was provided by the English, perhaps most strongly by Hill and his group at the Royal Marsden Hospital. The most consistent medical physics programs in research and in training of medical physicists in ultrasound has been that at the University of Wisconsin under Zagzebski, soon joined by Madsen. The overall Medical Physics program has produced approximately 220 Ph.D.s, most going into medical physics, the majority into academic or clinical work. A similarly strong history occurred later in Toronto, with the ultrasound part initiated by Hunt and Foster, with a good offshoot at the University of Western Ontario under a coauthor (A.F.). At the University of Colorado, a coauthor (P.C.) started an ultrasound medical physics effort under Hendee and in association with remnants of one of the original medical ultrasound groups, still headed by Holmes. Much of that effort moved to the University of Michigan and has continued for 27 years. Other notable groups in North America were active at Henry Ford Hospital and Wayne State University, e.g., Ref. 1, Thomas Jefferson University Hospital, e.g., Ref. 2, Temple University, e.g., Ref. 3, UCLA.[4] The University of Arizona with its major early, although not the earliest,[5,6] ultrasonic hyperthermia effort[7] helped spawn several current leading efforts (Harvard,[8,9] Washington University,[10] and UCSF).[11] Several groups and individual faculty based in physics departments have also contributed strongly to the field and the supply of medical physicists. Notable among those are at the Universities of Mississippi[12] and Vermont.[13]

The journal *Medical Physics* has contributed through scientific and educational publications; approximately 125 scientific papers on ultrasound have been published in the journal. The AAPM at its annual meeting has often had ultrasound scientific sessions and usually had educational ones. Ultrasound has been featured in several of its summer schools, e.g., Refs. 14 and 15, and reports.[16,17]

II. ACOUSTIC WAVE PROPAGATION

Mechanical vibrations of tissues at ultrasonic frequencies are propagated exceptionally well when the particle vibrations are parallel to the direction of propagation, producing longitudinal waves. Vibrations transverse to the direction of propagation, i.e., shear waves, are attenuated very rapidly in tissues other than bone. That is, tissues that can be sheared

easily, almost like a liquid. Nevertheless, low-frequency shear waves in the audible range can be followed by ultrasound to produce images of biological tissues. Those basics of ultrasound propagation are covered well in the many textbooks produced by medical physicists for the various ultrasound users,[18–21] and in more advanced texts.[22–24]

III. TISSUE PROPERTIES AND IMAGE ARTIFACTS

Ultrasonic interactions in tissues are at fortuitous levels to allow sensitive and high-resolution imaging of the tissues. This serendipity can be thought of in terms trying to design an ideal nonionizing radiation in which the attenuation in tissue (0.5 dB cm^{-1} MHz^{-1} for ultrasound) is not too great, the speed of propagation is rapid enough to allow rapid imaging (1540 m s^{-1} in soft tissues $\pm 6\%$), the wavelength is small enough (typically 0.1 to 0.8 mm) to allow high-resolution focusing, there is a high-contrast interaction property (e.g., at tissue interfaces) (preferably one working in a reflection mode requiring an unobstructed entrance window only from one side of the body), and all that at frequencies allowing inexpensive rf signal detection and processing.[25,26] The acoustic intensity changes occur at a macroscopic level, so ultrasound displays large tissue boundaries, i.e., edge enhanced imaging of major tissues. The changes also are at a subresolution level, so tissue structures also are distinguished by their backscatter coefficients. Quantitative data on the most important diagnostic property, the backscatter cross section or coefficient, is much less well studied and reported, although there has been some work,[27–29] including a great deal on methods of quantitative imaging of backscatter, to be discussed under tissue characterization.

The very high soft tissue contrast in ultrasound imaging comes at a cost, however. The large boundary (specular) reflection is very direction dependent and harder to interpret for imaging and therapy. The scattering as well as local absorption of acoustic energy is variable and greater than ideal, making shadowing and enhancement artifacts quite prominent in the images.[30,31] The attenuation artifacts are often diagnostic, but quite complex[32] due to the angle dependence, particularly of the large boundary scattering component. The speed of propagation differences far exceed those in ionizing radiation, leading to refraction and arrival time artifacts.[33,34] The typical asymmetric PSF also gives misleading results.[35] Coherent imaging in ultrasound allows higher spatial resolution than incoherent, but gives speckle noise and phase cancellation artifacts.[36] The basic properties of tissues as they relate to artifacts have been rather well studied and explained in the medical physics literature.[37,38] One most important artifact that has not been well studied is multiple scattering, which competes with clutter in the point spread function for filling anechoic structures with low-level echoes. Multiple scattering or reverberation artifacts are distinguishable from lateral and elevational clutter by their filling in a cyst from the direction of beam entry.[39]

IV. TRANSDUCERS AND BEAMFORMING

For a curved surface of an ultrasound transducer, the wave is launched normal to the surface at every point. For a transducer element shaped as a spherical section, a nearly ideal beam is launched toward a focal point, with some important limits due to diffraction.[40,41] Similar spherical and other focusing can be achieved with shaped radiators and lenses. With a single element transducer there is only one good focal point, so high resolution imaging or focused therapy must be accomplished by physical motion of the transducer, lenses, or reflectors. These approaches are slow and require relatively frequent maintenance.

With arrays of small transducer elements beams can be formed in a variety of shapes, described to a reasonable degree by summation of Huygens's wavelets from the centers of the elements. For element dimensions >1 wavelength (λ) in one direction the wave front from a single element falls off pretty rapidly as a function of angle from the normal to the element face, so strong focusing or large angle steering of the beam becomes impossible. Linear, phased, and curved linear arrays have single elements in the slice thickness direction, with quite weak focusing in that direction [focal length/diameter (F number) ~ 4]. For rapid sector scanning over large angles, phased arrays are used with element spacings of $\leqslant \lambda/2$ and the entire array is employed to transmit every beam, at least at the greater transmit focal depths. "Linear" and "curved linear" arrays typically have 1 λ element spacing that allows receive focusing with F number as small as 1.5, or modest, 20°, beam steering.[42,43] Transmit focusing is not as flexible as receive focusing in beamformed ultrasonic imaging. Once a transmit focus is chosen, then only a small range of depths (the focal zone) has a narrow beamwidth. To overcome this physical limitation, multiple transmit focuses are used for each line in the image. Such focusing has become quite complex.[44,45] One can transmit into a large or medium area and reconstruct well-focused transmit and receive beams at all depths using multiple transmit pulses[46–48] but there are time and signal to noise tradeoffs associated with these synthetic aperture techniques. 2D arrays are becoming available, initially for cardiac applications and using many tricks to keep the number of electronic channels similar to that in current systems, 128 to 256.[49,50]

Work on construction of 2D array transducers with large numbers of elements by integrated circuit methods began some time ago[51,52] and is now nearing initial fruition with capacitative micromachined ultrasonic transducers (CMUTS).[53,54]

V. SCATTERING FROM TISSUE AND TISSUE CHARACTERIZATION

Acoustic properties of tissues as measured over many decades were tabulated well by Goss and Dunn.[55,56] A quite complete and remarkably still relevant summary is included in the excellent book by Duck.[57] Most of that data was acquired *in vitro*, often fixed in formalin, and/or at room temperature. About the time of the Goss and Dunn reviews, efforts at quantitative imaging of ultrasonic interaction

properties *in vivo* was becoming quite popular under the title of "tissue characterization." It was warned that this title was too ambitious, suggesting that pathologic states could be identified unambiguously, that there would be a medical backlash when artifacts in those measurements and tissue variability defeated that lofty interpretation of the field.[58] Indeed, exactly that prediction was borne out in the mid 1980s, after which prominent use of the words "tissue characterization" in the rational statement of a grant proposal usually resulted in rejection of that proposal.

Important properties studied extensively to aid tissue identification (tissue characterization), as well as to aid artifact removal as described above, have included, for example, ultrasound attenuation coefficient,[59–63] speed of propagation, backscatter coefficient—its directionality and frequency dependence,[62,64–66] impedance,[67] nonlinearity parameter,[68–70] shear elastic modulus, and shear wave speed,[71–73] subresolution scatterer properties such as surface roughness,[74] scatterer size, and number density[75–78] and combinations thereof, other statistical properties of backscattered echoes, blood scattering,[79] ultrasound tissue characterization of bone,[80] and cellular imaging and tissue characterization with acoustic microscopy.[81] The effect of temperature was particularly strong, as was tissue fluid content, which varied strongly between *in vivo* and *in vitro* conditions. Early physics contributions to measures of careful tissue properties interoperatively included Refs. 82 and 83. Considerable effort was and continues to be directed toward quantitative imaging *in vivo.*

VI. IMAGING SYSTEMS

The last two decades have witnessed significant changes in ultrasound imaging systems. The first digital scan converter was developed by medical physicist Goldstein under NSF Grant GJ-41682. With the advances in computer technology and miniaturization, ultrasound systems have incorporated higher-end features in lower cost systems and systems have become smaller. With these advances, portable ultrasound systems with full features are now available. Examples of portable systems are manufactured by: Terason, which uses a full 128-channel system and consists of a laptop computer, a transducer, and a small processor box; and by Sonosite, which makes use of custom designed application-specific integrated circuit (ASICS).

A typical ultrasound system is generally composed of major components, which are described in the following sections. Ultrasound systems are explained in standard medical physics texts.[19,20] Most ultrasound textbooks generally are also for residents and technologists,[84] and some are for scientists and engineers.[22–24]

Each ultrasound system has a selection of ultrasound transducers typically designed for use at different frequencies and for specific applications, such as endo-cavity, vascular, abdominal, small parts, etc. imaging. Modern transducers are composed of piezoelectric linear or multielement phased arrays capable of producing images in real time. Most arrays are one-dimensional, typically with 128 or more elements. Since one-dimensional arrays have fixed focusing in the direction perpendicular to the array (elevation), some systems have additional transducer elements generating what is generally labeled as 1.5D arrays, allowing more flexibility in focusing in the elevational direction. Two-dimensional arrays are also now available in high-end systems allowing not only focusing in the elevation direction, but also real-time 3D imaging (i.e., 4D imaging).[85]

Typical system user interfaces makes use of a computer keyboard used to enter patient information, and custom buttons, knobs, and sliders used to control the operation of the system. Some systems make use of touch screens, obviating the need for a computer keyboard. In addition to input capability, the systems also provide means for connecting to a local area network for archiving of images and transmitting images to remote diagnostic stations.

The front-end electronics subsystem provides beamforming and signal-processing capability of the ultrasound machine. The transmit beamforming components organizes the signals to be sent to the transducer elements with proper timing. Echo signals received by the transducer are sent to an analog-to-digital converter and then organized by the beamformer to prepare the signals for generation of the ultrasound image. Thus, this subsystem includes signal-processing capability such as filtering and generation of signals for Doppler imaging.

The back-end electronics subsection receives the rf signals from the beamformer and generates the ultrasound image. This involves organizing the signals from the data lines through a scan converter into the proper raster scan format suitable for the computer or video monitor. Thus, this subsystem incorporates multiple functions, such as color and gray-scale mapping and compression.

The subsystems described above are controlled by a controller, which is composed of a computer or multiple microprocessors in modern systems. This subsystem interacts with the user interface and sets up the proper transmit and receive beamformer settings suitable for the selected transducer and the desired image settings.

Multimodality systems involving ultrasound are increasing in number and importance. They include thermoacoustic imaging,[86,87] of which photoacoustic imaging is a promising, most active area of research.[88–90] Ultrasound has been attached to CT scanners and surgical equipment for real-time guidance of interventions planned with CT. Ultrasound has been used with microwave, electrical, and diffuse optical imaging to guide reconstruction of those less deterministic imaging methods.[91,92] Combined ultrasound and mammography/tomosynthesis systems are described under breast imaging.

VII. DOPPLER AND OTHER FLOW IMAGING MODES

The Doppler effect is used extensively in ultrasound imaging and is a key capability of most ultrasound machines. The physical principles and use of the Doppler effect for investigating blood flow are covered in detail in many books and review articles. The technique is generally well under-

stood; however, progress and innovations are still continuing. The technique has progressed from simple continuous wave (cw) Doppler, which provided a sensitive method to measure blood velocity (component) but with the limitation of range ambiguity, to pulse wave (PW) Doppler, which overcame the range ambiguity limitation with range gating, to color flow imaging (CFI) techniques.[93,94]

Color flow imaging (CFI) was developed in the 1980s and provided a real-time blood velocity (component) and direction displayed in color superimposed on the gray-scale B-mode ultrasound image. This development represented a major advance in medical ultrasound and greatly extended its use in vascular and cardiac imaging. Typically, red is assigned to flow toward the transducer and blue away from it, with the color intensity increasing proportionally to the velocity. Since the velocity and direction must be calculated in multiple locations to cover a region of interest, the CFI image frame rate suffers. Thus, to increase the frame rate to observe fast events, the region-of-interest is reduced.

In the 1990s a variation of CFI was developed and was initially studied by a medical physics group and collaborating radiologists.[95] This development is usually called power Doppler imaging or ultrasound angiography. In this technique, only the Doppler signal power (or intensity) is displayed superimposed on the gray-scale B-mode image, with no velocity direction.[96] Since this technique is dependent on the integrated reflected power generated by moving red blood cells, it is more sensitive to flow than CFI and can produce a useful image of blood flow even close to 90° to the transmitted beam. The increased sensitivity of this technique allows imaging of small vessels and blood flow in tumors.

3D techniques have also been applied to both CFI and power Doppler imaging. One approach made use of a linear mechanical scanning mechanism to translate the transducer as Doppler color flow or power Doppler images was acquired by a computer and reconstructed into a 3D image. This 3D technique has been implemented in many vascular B-mode and Doppler imaging applications, particularly for carotid arteries and tumor vascularization. North American medical physics groups and the journal have been particularly active in this field.[95,97,98] Heart, and obstetrical applications have also been explored intensively.[37,99] Figure 1 shows several examples of linearly scanned 3D images made with a mechanical scanning mechanism.

Since the Doppler effect provides information on the component of the blood velocity relative to the ultrasound beam, the actual velocity vector information of the blood flow is not available. Thus, investigators have pursued the development of techniques that provide the true blood velocity and the direction of its vector. These techniques include velocity estimation using correlation,[100] wideband maximum likelihood,[101] and spatially separated Doppler transducers.[102]

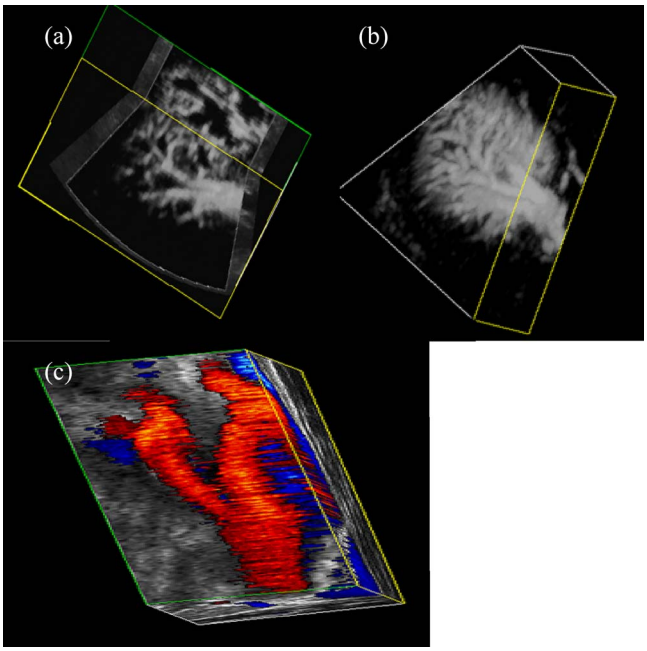

FIG. 1. Three-dimensional ultrasound images obtained using a mechanical scanning mechanism and shown using a cube-view approach. (a) B-mode image of a kidney; (b) power Doppler image of a kidney; (c) Doppler image of the carotid arteries, showing reverse flow in the carotid sinus.

VIII. NONLINEAR ACOUSTICS AND IMAGING

Linear acoustic propagation in a medium with respect to ultrasound would result if the shape and amplitude of the signal at any point in the medium were proportional to the input excitation. However, tissue exhibits a nonlinear property with respect to ultrasound propagation, resulting in the shape and amplitude of the acoustic signal changing as it propagates into the tissue. Specifically, ultrasound propagation in nonlinear tissue results in pulse and beam distortion, harmonic generation, and saturation of acoustic pressure. This is caused by the fact that, as a sinusoidal signal of a single frequency is generated and transmitted into a nonlinear medium, the signal will distort as it propagates because the compression phase velocity of the signal is greater than the velocity of the rarefaction phase. This effect will result in distortion of the wave as it propagates so that a "sawtooth" or "N"-shaped wave is generated, which has frequencies at harmonic multiples of the fundamental frequency. Since tissue attenuation increases with frequency, the higher harmonics will be attenuated, leaving an attenuated low-frequency signal at greater depths. Investigation of generation of harmonics in water by ultrasound imaging systems began in the 1970s and 1980s.[103–105] Use of nonlinear acoustics in medical imaging systems accelerated in the 1990s with primarily two applications: tissue harmonics and ultrasound contrast agents.

Tissue harmonic imaging was investigated in the 1990s by several groups.[106,107] and was commonly available in clinical ultrasound systems by the late 1990s. Two competing effects characterize ultrasound propagation in nonlinear media such as tissue. Increasing harmonics with propagation distance leads to increased absorption. The latter reduces pressure amplitude and harmonic generation. Since tissue heating is a consequence of absorption, nonlinear effects en-

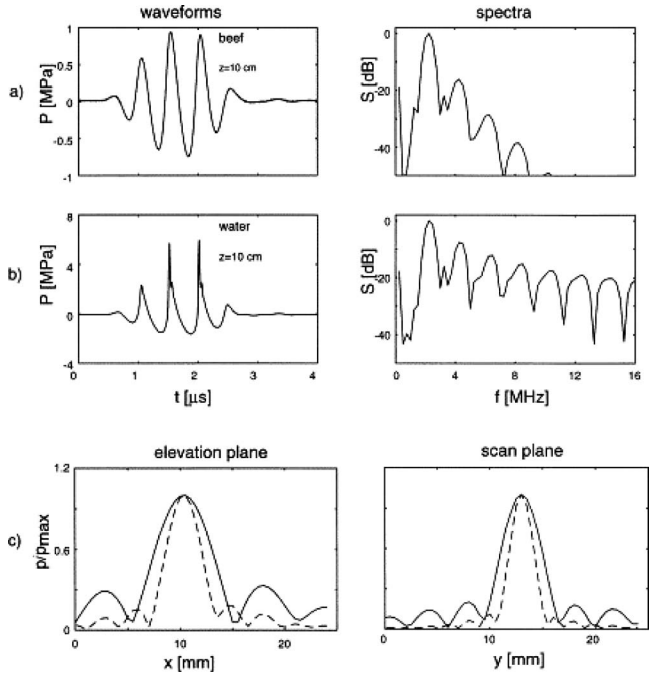

FIG. 2. Nonlinear propagation: (a) measured pressure waveform and spectrum of a 1.67 MHz sound pulse transmitted 10 cm through beef; (b) waveform and spectrum following transmission through water; and (c) measured focal beam profiles of the fundamental (solid lines) and nonlinear second harmonic beams (dashed lines). Since harmonic amplitudes are proportional to the square of the fundamental pressure, the wave passing through the relatively unattenuating water generates a disproportionate increase in the second harmonic, compared to that passing through attenuating muscle. The harmonic beam has a narrower main lobe and weaker sidelobes than the fundamental beam. From Burns, Ref. 111.

hance tissue heating as compared to the heating that would have occurred at the fundamental propagation frequency.[108,109]

Tissue harmonic imaging is typically implemented by filtering out the fundamental ultrasound frequency of the received beam. Second harmonic images have been shown to often improve contrast and resolution as compared to images generated by the fundamental frequency. These advantages result from multiple improvements, such as narrower beamwidth, reduced sidelobes, reduced reverberations and multiple scattering, reduced grating lobes, and increased dynamic range.[107,110] This is primarily due to the fact that these unwanted signals are mainly incoherent and are small in amplitude. Thus, they do not generate harmonics and can be filtered out in the second harmonic image.[111] In addition, since harmonics are proportional to the square of the fundamental pressure, increasing the acoustic input pressure will generate a disproportionate increase in the second harmonic, compared to the situation in which the medium is linear and no harmonics are generated (Fig. 2).

Elasticity and shear wave imaging is a natural application for ultrasound imaging, given the latter's coherence and ability to track small motions, particularly in the direction of ultrasound wave travel. Once again, efforts at quantitative imaging, e.g., nonlinearity parameter and tissue harmonic imaging, perfusion and power mode Doppler imaging, backscatter coefficient, and improved gray-scale imaging, have paid off most directly in converting the measured quantity[112,113] into an imaging one,[114,115] usually nonquantitatively. Tissue firmness to the touch has always been a major diagnostic tool. The modulus of elasticity or simple durometer testing has shown the information to be there with very high contrast. Ultrasound and MR imaging with dynamic and quasistatic[115–118] displacements have followed with good success, although plagued by many artifacts due to the simplified assumptions and that the imaging of elasticity instead of strain must contend with noise of an additional derivative.[118] The shear elastic modulus is responsible for perceived hardness and can be approached by imaging shear wave propagation with ultrasound or MRI, where the shear waves can be generated at locations of interest by radiation force at the focus of an ultrasound beam.[73,119] Very localized displacements can be produced and elasticity imaging accomplished in the vicinity of laser and acoustically produced, acoustically driven microbubbles.[120,121] The literature on techniques and applications is too extensive to cover here, but the contributions of the Wisconsin medical physics group are notable.[122,123]

Ultrasound contrast agents: Developments and applications of ultrasound contrast agents have been intensely investigated throughout the world, but less so in the USA, where their approved range of applications is extremely limited. Quite restrictive contraindications and monitoring requirements were placed on the use of ultrasound contrast by the FDA, but those were relaxed substantially quite recently.[124] Hopefully the range of approved applications will also be broadened. Most ultrasound contrast agents are encapsulated gas-filled bubbles ($1-10\ \mu$m) that are intravenously injected. Here, we summarize the nonlinear effects related to microbubbles, but for information on the physics and imaging applications related to gas bubbles, the reader is referred to recent reviews.[125,126] The strong scattering of resonant bubbles was recognized early and medical physicists contributed in their acoustic characterization.[127,128] In the presence of an acoustic field, microbubbles act as highly nonlinear resonators. For acoustic fields with a low pressure, the bubbles undergo forced vibrations and can keep up with the fluctuating pressure field—linear resonance. However, as the pressure is increased, they can expand with the rarefaction phase, but cannot contract without limit due to the encapsulated gas. Thus, as determined by a leading ultrasound physicist,[129] the bubbles' pressure expansion and contraction response is asymmetric, resulting in harmonics and other behavior of highly nonlinear scatterers of ultrasound.[130] In harmonic imaging with contrast agents, the signals at fundamental frequency primarily generated from tissue are suppressed, allowing imaging of the scattered signals at the second harmonic, as studied extensively by Burns,[131,132] an import from English medical physics training. Since the passband of the transmit signals at the fundamental frequency and the passband of the receive signals at the second harmonic may overlap, the large linear signal from tissue may mask the harmonic signal from the small quantity of contrast agent. Thus,

transmit and receive signal bandwidths should be narrow, reducing axial resolution. The trade-off between contrast and resolution in contrast imaging leads to the use of increased transmit intensities, in which micro-bubble destruction can occur, resulting in reducing imaging frame rate to maintain detection sensitivity.[133] Techniques to overcome these limitations are being investigated and innovations involving power-dependent and pulse-inversion techniques are being developed.[134] 3D quantitative imaging of mean vascular transit time and perfusion with ultrasound contrast agents has been time consuming.[135] The step to 3D contrast enhanced physiologic imaging is critical to realize the clinical potential, and some progress has been made.[136]

IX. SPECIALIZED SYSTEMS AND APPLICATIONS DEVELOPMENT

IX.A. Breast imaging

Breast imaging with ultrasound is a special case because of the emphasis it has received and the opportunities for innovation. Since the early days of ultrasound imaging, breast cancer detection and diagnosis has been a target application and one emphasized by medical physics researchers.[137–140] Breast motion during the mechanical scanning as well as lower ultrasound frequencies, fixed focus and mechanical instability of the compound imaging articulated arm[141] produced much lower resolution than was achieved subsequently. It was rather clear that ultrasonic discrimination of cysts was quite complementary to information from mammography, a fact that continues to be confirmed with more advanced systems and techniques.[142,143]

Pushing a relatively small, 1D linear array close to the lesion without concern for displaying the entire breast enabled the use of higher frequencies. That, along with dynamic electronic focusing on reception and multiple transmit foci with larger apertures, allowed higher resolution and sensitivity. Such arrays are still the current state of clinical practice. Color flow imaging and other Doppler studies have been performed extensively by medical physicists and others as a possible discriminator of breast cancer.[144,145] Breast cancers are, in general, more vascular, with somewhat distinctive patterns, and their vascularity can contribute to the diagnosis. However, it is still controversial as to whether the improvement is worth the added time of performing a Doppler study.

Automated and other 3D imaging: 3D imaging of the breast offers substantial potential advantages because of the more consistent coverage and better statistical sampling of features such as border characteristics, shape, and vascularity. Approaches have included major commercial efforts to establish ultrasonic breast cancer screening in the U.S. with water path scanners in the early 1980s. These efforts failed to convince the medical community. Free-hand 3D scanning allowed higher frequencies with less aberration and is often used now without position encoding in the slice thickness (elevational) direction to record entire regions of interest. With encoding of the elevational motion, the potential of whole breast imaging is increased. Reproducibility of positioning is not as good as in most organs, particularly for supine scanning, where the breast tissues are spread out by gravity to maximize imaging depth and therefore greatest usable frequency and control of artifacts. Ultrasound imaging in the compressed mammographic geometry allows better correlation of lesions and other structures between the ultrasound results and those of mammography.[146–148] This geometry probably can provide more complete coverage of breast tissues than imaging with water paths in coronal planes (breast axial planes), as is done for ultrasonic CT and dedicated breast x-ray CT, but worse coverage than free-hand scanning in the supine position.

Ultrasonic CT (UCT) allows detection of transmitted and forward scattered ultrasound as well as backscatter. UCT was studied extensively in the late 1970s and early 1980s,[138,149–159] but was caught in the decision of the U.S. medical community that ultrasound breast cancer screening and quantitative imaging (tissue characterization) were not productive or were premature. This setback is being overcome only in the last few years, with a resurgence based on new technologies and steady science. The large 360° aperture available in scanning the dependent breast in horizontal planes allowed many advanced imaging schemes based on corrections for, or imaging of, diffraction and variable propagation speed.[137,149,152,153,159–161] Much of the most advanced work has been done with the assumption of cylindrical geometry, using full ring array transducers,[162] now with reasonable focusing in the slice thickness direction. The latest versions of these approaches are producing rather good results for attenuation, speed of sound, backscatter, and other interaction images, but there are substantial artifacts, particularly in the attenuation images. An alternative approach is a simple transmission array and a 2D receiving array that rotates fully (Techniscan Med. Syst., Salt Lake City, UT).[163]

There have been quite a few efforts to develop and test systems of automated 3D US in a mammographic geometry[164–167] in both a combined system and in separate systems. One such system, while successful in finding all the cancers, missed smaller benign masses. The study was stopped due to the breast slipping out of compression due to the slippery coupling gel and due to limited visibility of lesions near the nipple and chest wall.[168] One stand-alone device approached commercialization in the mammographic geometry, but was changed to the simpler supine scanning geometry.[169] Others claim to have found ways to ameliorate compression and coupling problems and achieve the important goal of direct spatial colocalization of structures in mammographic and DBT images with automated ultrasound images.[170]

IX.B. Brain imaging

While transmission of focused ultrasound through the skull poses significant problems, trans-skull ultrasonic propagation for diagnosis and therapy has been investigated for several decades. The use of trans-skull ultrasonic imaging has primarily been directed at transcranial Doppler to detect blood flow in some cerebral arteries or lack of blood flow

due to emboli from the heart or carotid arteries. In the past few years, the use of transcranial ultrasound for therapeutic application has attracted significant interest based on and leading to a number of novel applications, such as acoustic tomography,[152,171,172] targeted drug delivery and blood-brain barrier disruption,[173] cerebral arteries blood flow,[174] thermal tumor treatment,[175] and use of transcranial ultrasound in ischemic stroke therapy,[176] all discussed subsequently.

Therapeutic applications rely on the use of focused ultrasound to create well-delineated regions of energy deposition via high-frequency mechanical oscillations of tissue. Key to therapy applications is the ability to localize the delivery of energy to a well-delineated region. However, the skull is not a simple medium with a single thickness and speed of sound. Rather, the skull varies in thickness, density, acoustic absorption, and speed of sound, resulting in deformation of the path of the longitudinal transmitted sound. These properties create difficulties in focusing the acoustic field and delivering the planned energy to the desired region. In addition, the high acoustic absorption of the skull limits the amount of energy that can be delivered.

Investigators have attempted to solve the problems associated with propagation of longitudinal acoustic waves through the skull by correcting the phase and amplitude of the transmitted sound. Some approaches have used multiple acoustic sources. By correcting the relative phase and amplitude generated by each source, it is possible to produce a well-delineated pressure field inside the brain.[177,178] This can be accomplished by obtaining detailed information on the morphology of the skull region used for transmission of the acoustic energy. Using geometric and compositional information, a sound propagation model can be used to plan the phase and amplitude correction needed to produce the desired focused field in the brain.[179] The required information can be obtained using MR imaging[178] or CT. With 2D arrays offering independently addressable elements on transmit and receive,[180,181] or possibly with a chaotic cavity,[182] aberration correction will be obtainable with ultrasound.

Longitudinal acoustic trans-skull transmission has been used for a few decades with various degrees of success. More recently, shear wave transmission has been explored in an attempt to circumvent some of the problems facing longitudinal transmission. When an ultrasonic wave traveling in water arrives at the skull interface, a longitudinal reflected wave, a longitudinal transmitted wave, and a shear transmitted wave are generated. At an incident angle of 25° or larger, only a shear wave is transmitted. Since the speed of sound of shear waves in skull is close to the speed of sound in water and brain tissue, distortions of this wave are less severe than with longitudinal waves. Although distortions due to skull density and variation of thickness are less severe with shear wave transmission through the skull, skull attenuation of shear waves is greater than longitudinal wave attenuation. Nevertheless, applications making use of shear wave transmission that do not require delivery of high energy levels show promise and are being explored by a number of investigators.[183] These applications include brain-blood-barrier disruption, mentioned above,[184,185] tissue destruction using cavitation,[186] and heating using bubbles[187] (Fig. 3).

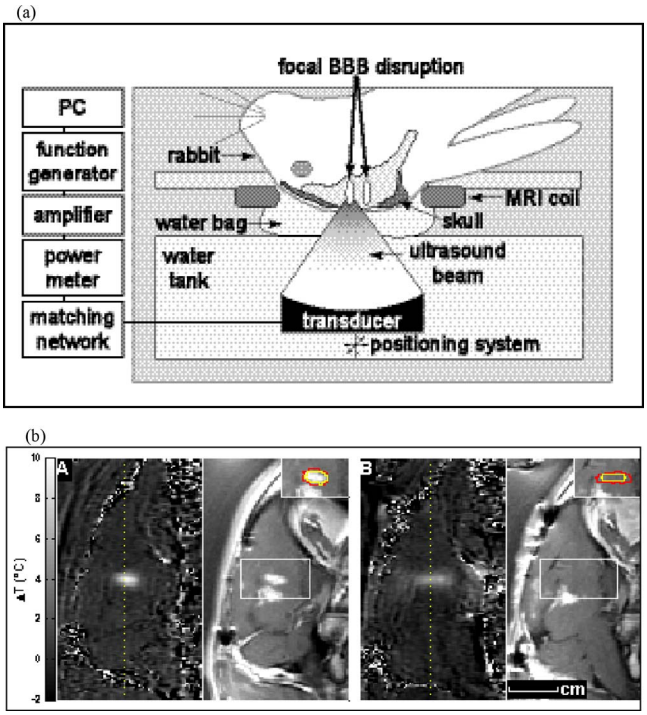

FIG. 3. (a) Experimental apparatus used to generate the results in (b), which shows the MRI-based temperature maps (left) and contrast-enhanced T1-weighted images (right) of two sonications in two rabbit brains with (A) and without (B) preinjection of Optison®. Isotherms drawn at 3 and 4 °C are superimposed on the T1-weighted images in the insets. With Optison®, the length of the focal zone was reduced, and the heating was centered at the focal plane (dotted line in the temperature images). The images were acquired parallel to the direction of the ultrasound beam. Note that in both cases a second location inferior to the first was also sonicated. In these images, the ultrasound beam propagated in a direction from left to right. (A: 1.2 W/10 s, 2.8 MPa, pulsed; B: 3n W/10 s, 4.4 MPa, CW). From Hynynen, Ref. 185.

IX.C. Small animal and early stage molecular imaging

Imaging of small animals *in vivo* requires resolution better than 200 μm, which yields anatomical detail comparable to clinical imaging of humans.[188] Thus, the use of ultrasound in imaging of small animals requires that the systems use center frequencies higher than 20 MHz. However, the use of high frequency imaging needed to obtain high resolution limits the penetration depth due to increased attenuation with frequency, and limits the field-of-view compared to high-resolution micro-CT or micro-MR. In addition, the usual limitation related to the inability to image bony and air-filled anatomy limits applications to imaging of soft tissues. However, the flexibility, real-time imaging capability, and low cost of high-frequency ultrasound imaging systems have stimulated developments and many applications in their use for preclinical investigations making use of small animal research models. These have been stimulated by the release of a commercial microultrasound imaging system (VisualSonics Inc., Toronto, Canada).

Applications in cancer research were among the first identified for microultrasound,[189] and the use of Doppler imaging at high frequencies allowed investigations of tumor microcirculation mapping.[190,191] Analysis of the radio-frequency spectral parameters allowed investigations of apoptosis, as well as investigations of different tumor microstructure characteristics.[192,193]

While 2D B-mode microultrasound imaging provided a valuable tool in cancer research, 3D imaging capability was shown to offer important advantages.[194] Thus, investigators have begun to extend the use of micro-ultrasound imaging to 3D by mounting the transducer on a mechanical motorized mover and collecting parallel 2D images separated by a computer controlled spacing.[195–197] Typically, the images were separated by 50 μm, requiring 200 images to cover 5 mm. This approach allowed accurate measurements of irregular shaped regions and accurate estimates of tumor volume required in monitoring tumor progression and regression.[195–197] Three-dimensional imaging also allowed viewing of anatomy in any orientation including views not possible using 2D imaging. This capability improved the ability to validate the developments of biomarkers of disease in preclinical studies of cancer and atherosclerosis,[198–200] and allowed detailed investigations into the neoangiogenesis process in animal tumor models (Fig. 4).[201] Microvascular elasticity imaging also is promising.[202]

Microultrasound also provides an important tool for the study of embryo development in the mouse. The use of 40–50 MHz microultrasound imaging has provided sufficient resolution to examine the development of the heart in a mouse from early embryonic to later neonatal stages.[203,204] In addition, real-time imaging at high resolution with high-frequency ultrasound has also allowed investigations into placental circulation in mice[205] and analysis of lethal and nonlethal dilated cardiomyopathy in mutant mice during the first week after birth.[206]

During the last decade, important advances have advanced the use of microbubble contrast agents, which allows lesion perfusion analysis with a sensitivity comparable to CT and MR. For a current summary of this field, the reader is referred to a review by Ferrara *et al.*[125] The use of microbubble contrast agents in preclinical studies is expanding rapidly, particularly with the development of techniques used to conjugate bubbles to ligands that cause them to adhere to receptors such as VEGFR, allowing investigations of angiogenesis and inflammation.[207,208]

X. PERFORMANCE EVALUATION

Ultrasound system quality control and performance evaluation has been studied and developed rather extensively, although the demand for routine services has not been as great as with more regulated imaging modalities. The first standard for testing of ultrasound imaging systems was the AIUM 100 mm Test Object.[209] Compared with a wire-holding frame in an open water bucket, this device offered in one of its forms the convenience of an enclosed water tank for off the shelf use with ease of alignment of the image plane with internal wires. The Southwest Regional Center for Radiological Physics, Hendee, P.I., funded by NCI and administered through the AAPM, provided the first national program for education in ultrasound system QC, performance evaluation, and safety. Wires in water were replaced by tissue-mimicking phantoms developed in the medical physics department at the University of Wisconsin[210] and their approach has dominated the market for several decades. Water loss over time is a problem but alternatives have similar problems, limited applications, or inconvenience.[211,212] Numerous standards and guides for ultrasound QC and higher-level performance evaluation have been produced nationally and internationally by organizations with strong participation by medical physicists, e.g., Refs. 16, 17, and 213.

XI. ULTRASOUND-INDUCED BIOEFFECTS

Because of the high acoustic pressures involved and previous experience with other medical imaging and therapeutic radiations, patient safety and the potential for therapeutic use has been an important issue from the beginning of medical ultrasound research. The research and guidelines for safe use are summarized regularly.[214–217] One of the largest uncertainties is probably estimation of the exposure level *in situ*, because of the large and highly variable attenuation of ultrasound. This uncertainty has been addressed by simple[218] and more complex models[219] and by difficult measurements in humans *in vivo*.[220] These guidelines have been directed toward imaging in the typical diagnostic range of 1–15 MHz, but higher frequencies do not raise special concerns as long as thermal effects are considered appropriately. Thermal effects on the embryo/fetus of diagnostic ultrasound have been a topic of strong interest, but training and real-time output display requirements[218] persuaded the FDA to raise general purpose ultrasound output guidelines for 510(k) approval to the higher cardiovascular limits. This move probably has resulted in better and more versatile ultrasound systems, but there are not large safety margins. Apparently negligible damage can be done to microvasculature by ultrasound at the lung surface at the highest outputs,[221] as can extremely focal vascular leakage from bubble oscillations in high-amplitude ultrasound fields.[222] The only known location of a potentially substantial effect is in the kidney, where the high blood pressure gradients can cause enough hemorrhage for loss of the nephron.[223]

XII. ULTRASONIC EXPOSIMETRY, ACOUSTIC MEASUREMENTS, AND SAFETY STANDARDS

The study of methods for measuring exposure levels, and their relationship to possible biological effects, accelerated as ultrasound became the dominant method of imaging the fetus and was used even in normal pregnancies. Resulting exposimetry methods are reviewed regularly.[224,225] Ultrasound exposures from commercial imaging systems have been reported rather extensively.[103,226] Requirements for reporting relevant output of commercial systems[227,228] kept up with or exceeded those for x-ray imaging and the requirement for real time, on-screen reporting of estimated biophysically rel-

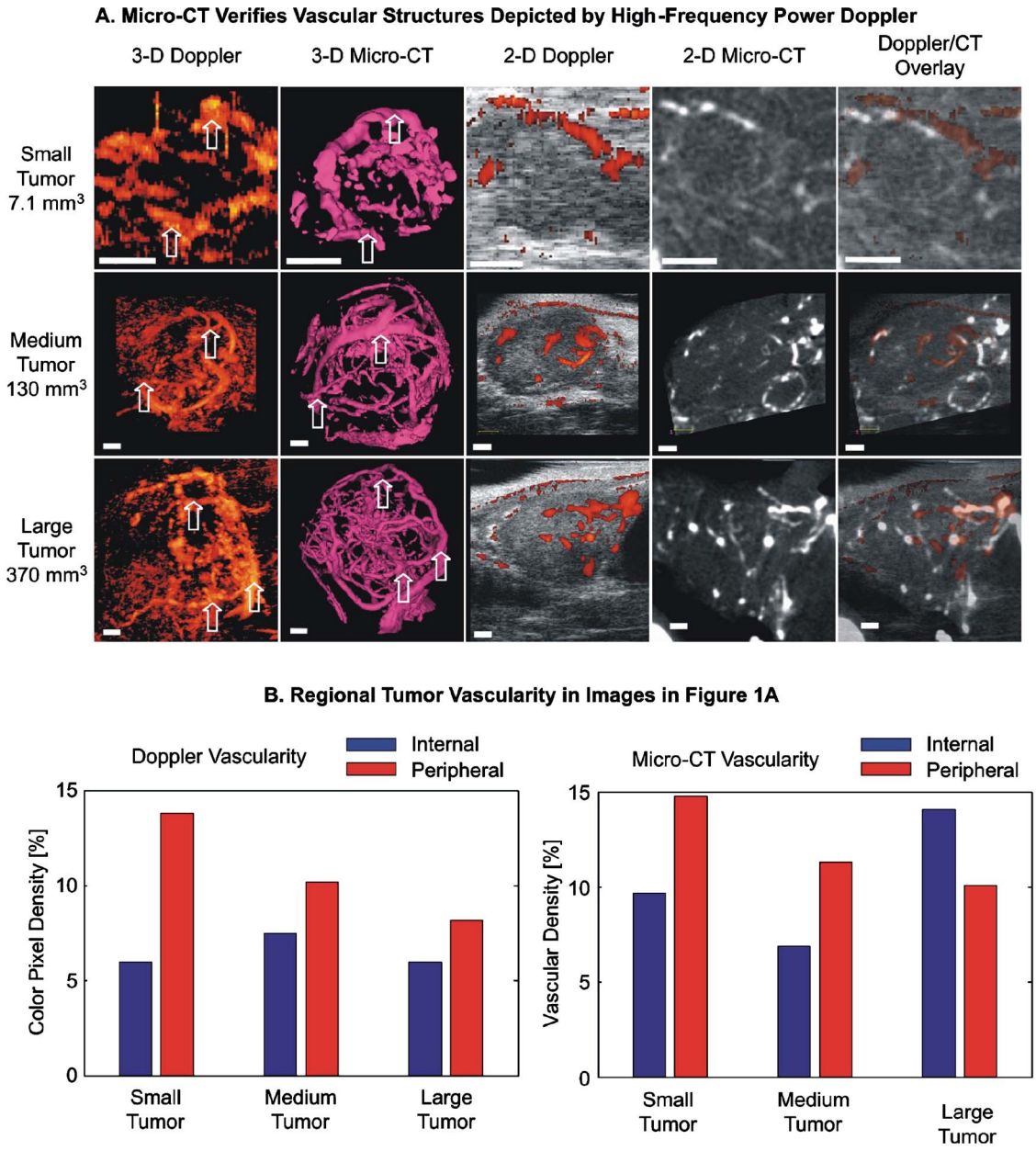

FIG. 4. Power Doppler ultrasound images of vasculature in a GEM-prostate cancer model are verified by Microfil-enhanced micro-CT. (A), from left to right in the first row, a three-dimensional power Doppler image, a three-dimensional micro-CT image, a two-dimensional plane from the three-dimensional power Doppler image, the matching two-dimensional plane from the three-dimensional micro-CT image, and an overlay of the two-dimensional power Doppler and micro-CT images of a 7.1 mm^3 tumor. Second and third rows, equivalent sequences of images from a 130 mm^3 tumor and 370 mm^3 tumor, respectively. Arrows, sites used for registration of corresponding vessels. Bars, 1 mm. (B), bar graphs of internal and peripheral vascularity estimated from the three-dimensional power Doppler and micro-CT images shown in (A). The power Doppler and micro-CT vascularity metrics (CPD and vascular density, respectively) are shown on separate graphs. Adapted from Xu *et al.* (Ref. 201).

evant parameters *in vivo* have lead the medical imaging field.[218,229]

XIII. ULTRASONIC THERAPY

The topic of ultrasonic therapy and the role of medical physics therein is too large to cover adequately in this review, but some pointers to the literature will be given, including recent reviews.[230] The most effort has been on hyperthermia for cancer treatment. There is a therapeutic advantage for thermal treatment of tumors with high metabolic rates and often poor thermal protective mechanisms. However, it is hard to maintain the temperature in a narrow window for an extended period of time, particularly for large treatment volumes. More effort has been directed in recent years to thermal and mechanical (cavitational) ablation. A method of very high-amplitude ablation, histotripsy, is particularly promising. Here, clouds of cavitation bubbles are initiated and carefully controlled with relatively low heating

Hyperthermia and tissue ablation are referred to in the term high-intensity focused ultrasound (HIFU). This acro-

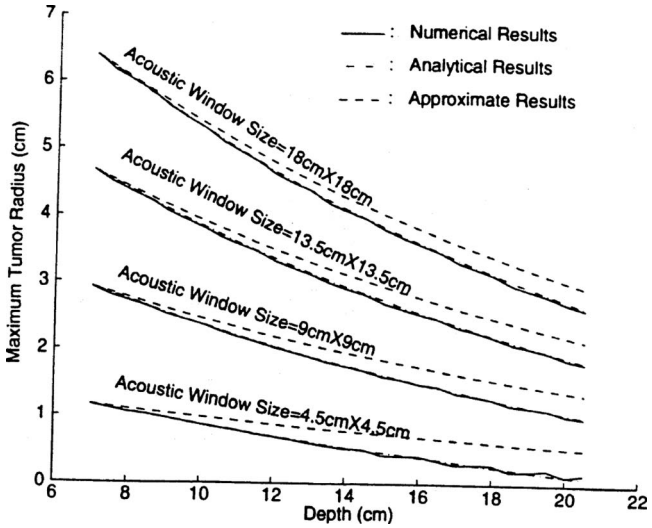

FIG. 5. Maximum treatment volume size allowed by heating of overlying tissues as a function of tumor depth, various body aperture sizes, given typical tissue properties. Adapted from Ref. 231.

nym refers to a technique wherein focused ultrasound beams are emitted from a high-powered transducer that can target a tissue volume inside the body. The energy deposition causes a sharp temperature increase within the focal volume, resulting in tissue coagulation, necrosis, and the elevation of localized tissue stiffness. Two principal mechanisms, tissue heating and acoustic cavitation, are responsible for HIFU-induced tissue damage. Each mechanism enhances the other. HIFU systems commonly operate in a frequency range of 0.5–5 MHz, generating focal high-level intensities in a range of $<1000-10\,000$ W/cm^2 that cause irreversible cell destruction and protein denaturing in seconds.

HIFU treatment is noninvasive and nonionizing, which means it can be repeated as desired, having no long-term cumulative effects when performed accurately. It increases tissue temperature in the focal area up to 60 °C for temperatures to as high as 100 °C in seconds, which is sufficient to induce thermal coagulation while minimizing blood perfusion effects. However, potential limitations to the current clinical application of HIFU still exist, such as the long treatment time with large tumor, deeply located tumors. Due to the total power attenuation through the intervening tissue, there exists an upper bound of treatable tumor volume at a given depth. The relationship between the therapeutic volume and tumor depth is shown in Fig. 5.[231] In some cases, patients complain about local pain after HIFU therapy, which may be caused by normal tissue overheating, although this is not terribly common. Periosteal pain can be severe and is a challenge because of the rapid heat deposition of ultrasound in bone.[232] The diaphragm, lung, bowel, and other gas-bearing tissues are likely targets for cavitational and thermal damage.[219]

The initial applications of HIFU on biological tissues were proposed by Lynn *et al.*[233] in 1942. Later, Burov[234] suggested using HIFU to treat malignant tumors. The bioeffects and specific properties of focused ultrasound on tissues were investigated in further studies.[5,56] As mentioned earlier, the group at the University of Arizona[7,235] trained many people in therapeutic ultrasound who have established and enhanced programs throughout the country, including several in medical physics programs. In the last two decades, the potential of HIFU for clinical use has been enhanced greatly by combining HIFU treatment with MRI guidance.[236] Image guidance by ultrasound or other modalities,[237,238] allows reasonably accurate HIFU dose delivery to the target tissue with minimal damage to the overlying and surrounding normal tissue. Imaging modalities also play an important role in treatment follow-up by means of the treatment efficacy, early recurrences, and therapy-induced complications.

Histotripsy offers the potential of tissue ablation without substantial heating of overlying tissues, as the violent activity of a microbubble cloud in an intense ultrasound beam liquefies the tissue to the subcellular level.[239] Extremely precise surgery can be performed transcutaneously with this technique in accessible locations. The treatment can be monitored easily with conventional ultrasound imaging.[240] However, treating large volumes at present still requires substantial time to avoid unacceptable heating of overlying tissues.

Drug delivery,[173] clot disruption,[241] accelerated healing,[242] and hemostasis of vascular injuries[243] and incisions[244] are among many advanced therapeutic applications of ultrasound.

XIV. THERAPY TREATMENT PLANNING AND GUIDANCE

Development of ultrasound for treatment planning was ongoing some time ago.[245] Ultrasound has been studied and developed and used qualitatively and quantitatively to evaluate response to chemotherapy[246] and various experimental drugs.[247] Prostate therapy has been a leading application of ultrasound for treatment planning because of its accessibility for ultrasound imaging and the utility of nearly real-time feedback. This application is treated in detail as an example.

XIV.A. Prostate therapy treatment, planning, and guidance

The most common treatment regimens for clinically localized prostate cancer are watchful waiting, radical prostatectomy, external beam radiation, and brachytherapy. While watchful waiting is appropriate for some, the majority of men diagnosed with early stage cancer will request or need treatment. While very effective, radical prostatectomy does entail some significant morbidity (incontinence and impotence). Although various prostate treatment techniques have been developed and investigated over the past decade, e.g., brachytherapy, cryosurgery, hyperthermia, interstitial laser photocoagulation (ILP), and photodynamic therapy (PDT), external beam radiotherapy and brachytherapy are still common. These techniques have benefited greatly from advances in ultrasound imaging technology and techniques.

XIV.A.1. Ultrasound imaging in external beam prostate radiotherapy

Advances in external beam radiotherapy techniques have generally resulted in improved precision and accuracy in the delivery of radiotherapy, allowing better control of the dose distribution within the target and sparing normal tissues. These techniques require better methods to delineate the prostate boundaries as well as improved methods to monitor prostate motion.[248] Various imaging techniques have been applied to high-precision prostate radiotherapy, including ultrasound imaging.

Transabdominal ultrasound imaging has had an important impact in daily prostate localization before treatment,[249] and several ultrasound-based systems have been developed for image-guided radiotherapy. In these systems, the ultrasound transducer is typically localized with respect to the treatment isocenter, and its 3D position is measured. By calibrating the system, the location and orientation of the ultrasound images can then be referenced to room coordinate system, and hence the location of the prostate can be localized in 3D and referenced to the treatment isocenter.[250] In these prostate localization systems, the transabdominal ultrasound transducer is held by the operator, and the transducer's position and orientation is tracked using an external tracking device, e.g., articulated arms,[251] infrared tracking,[252] camera-based optical tracking with 3D ultrasound imaging, and real-time ultrasound monitoring.[253] A specialty 3D ultrasound imaging system is available for breast and prostate radiotherapy (Resonant Medical, Montreal, Canada).

XIV.A.2. Transrectal US (TRUS)-guided permanent implant prostate brachytherapy

Prostate brachytherapy is a form of radiation therapy in which about 80 to 100 radioactive seeds (e.g., ^{125}I or ^{103}Pd) are placed permanently into the prostate.[254,255] Because the control rates of prostate cancer appear to be dose dependent, it is theorized that the higher doses produced by brachytherapy will yield higher control rates than external-beam radiation without a rise in complications. In the past decade, removable implant techniques have been developed and used in some institutions. In either technique, in order to deliver a high conformal dose safely to the prostate, radioactive sources must be positioned accurately within the gland, which can be accomplished using ultrasound guidance.[256,257]

Transrectal US guidance (TRUS): Real-time TRUS guidance for prostate brachytherapy was introduced by Holm in 1981 (Ref. 258) and refined by Blasko and Grimm, increasing its popularity.[259,260] Currently, the most common approach makes use of a TRUS-based preimplantation dose plan (preplan) to determine the total activity and distribution of the radioactive seeds in the prostate. At a later outpatient visit, the seeds are implanted under general or spinal anesthesia using TRUS guidance, while the patient is placed in the "same" lithotomy position as the preplan. At a later separate patient visit, the actual seed locations are determined with CT or fluoroscopy and a postimplantation plan (postplan) is generated.[261] If errors are detected (e.g., "cold spot"), then additional seeds may be added, but seeds cannot be removed.

Typically, a biplane TRUS transducer is used, which contains a side-firing linear transducer array and a curved array positioned near the tip producing an axial view perpendicular to the linear array. The probe is covered with a water-filled condom to allow good contact with the rectal wall, inserted into the rectum and attached to the brachytherapy assembly, which includes a needle guidance template and a manual stepper. The template guides the needles into the prostate in rectilinear and parallel trajectories, limited by the pattern of holes and positioning of the template.

Dose planning: For preimplant dose planning (preplan), the US transducer is typically withdrawn in 5 mm steps, while a 2D image is acquired at each step, resulting in about 7 to 10 2D transverse images. Typically, the margins of the prostate in the 2D images are contoured manually with a mouse and used in the treatment optimization software, which yields source positions for target coverage.[256,260]

Implantation: During the implantation phase, the patient is positioned in a similar orientation to the preplanning position. Once the TRUS transducer is in position, needles are inserted under TRUS guidance. Since the needles are often deflected during insertion, 2D TRUS visualization helps to detect the deflection. If the deflection is significant, then the needle is reinserted.

Recent advances: 2D TRUS-guided prostate planning and implantation has been extended to include significant advances such as 3D ultrasound[262,263] robotic aids,[263–266] dynamic reoptimization, needle tracking,[267,268] and seed segmentation from ultrasound images.[269] This type of approach permits planning and implantation at the *same session*, thereby avoiding problems of repositioning, prostate motion, and prostate size/contour changes between the preplan and the implantation. These improvements in the procedure have made use of advances in ultrasound imaging along 2 fronts: 3D prostate ultrasound imaging, and semiautomated prostate contouring in ultrasound images.

XIV.A.3. 3D TRUS imaging

3D TRUS systems[270] can make use of a side-firing linear array transducer, which is coupled to a rotational motorized mover.[271,272] The mover rotates the transducer around its long axis over a rotation angle of about 100° to generate a sequence of 2D images arranged in the shape of a fan.[262,273,274] As the transducer is rotated, 2D US images from the US machine are digitized at typically 0.7° intervals at 30 or 15 Hz by a frame grabber and stored in the computer. The 2D images are reconstructed into a 3D image while the 2D images are being acquired, allowing immediate viewing of the 3D image.[271] Figure 6 shows an example of the quality of 3D TRUS prostate images that can be achieved.

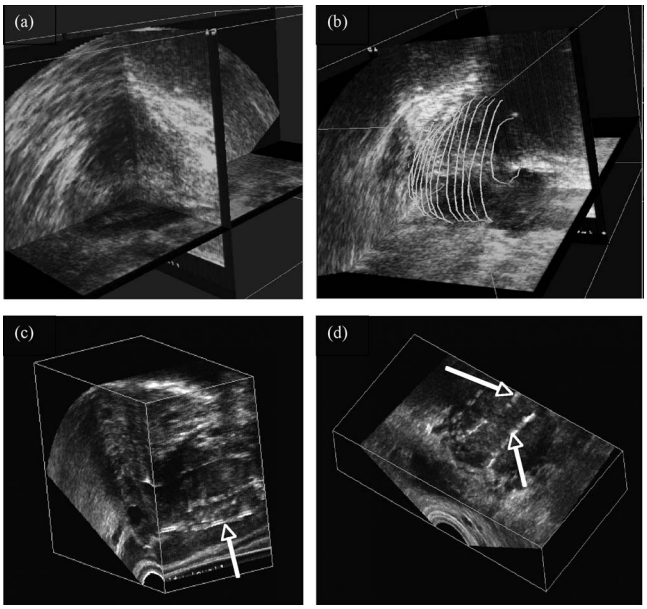

FIG. 6. Three-dimensional prostate images obtained with a TRUS ultrasound transducer coupled to a mechanical rotational scanning mechanism. (a) 3D TRUS image with three orthogonal views; (b) the 3D TRUS image of the prostate has been segmented; (c) 3D TRUS image of a brachytherapy patient obtained after the procedure. The image has been sliced to reveal rows of brachytherapy seeds (arrow). (d) The same image as in (c) but sliced in the coronal plane (not available using conventional TRUS imaging) revealing three rows of brachytherapy seeds (arrow). Adapted from Ref. 272, Fenster *et al.*

XIV.A.4. 3D Prostate segmentation

Since outlining the prostate margins manually is time-consuming and tedious, a semi- or fully automated prostate segmentation technique is required that is accurate, reproducible, and fast.[275] Because 3D US images suffer from shadowing, speckle, and poor contrast, fully automated segmentation procedures result, at times, in unacceptable errors. Over the past decade, many investigators have developed automated and semiautomated segmentation approaches, and some are now available in clinical TRUS-based prostate brachytherapy systems.

In one approach, the prostate is segmented in a series of cross-sectional 2D image slices obtained from the 3D TRUS image, and the resulting set of boundaries is assembled into a single 3D prostate boundary.[276,277] The method consists of three steps: (i) The operator manually initializes the algorithm by selecting four or more points on the prostate boundary in one central prostate 2D slice. A curve passing through these points is then calculated and is used as the initial estimate of the prostate boundary. (ii) The curve is deformed using a discrete dynamic contour algorithm until it reaches equilibrium. If required, the curve can be edited by manually repositioning selected vertices. (iii) The 2D segmented prostate boundary in one slice is extended to 3D by propagating the contour to an adjacent slice and repeating the deformation process. This is accomplished by slicing the prostate in radial slices separated by a constant angle (e.g., 3°) intersecting along an axis approximately in the center of the prostate.[277] The accuracy of the prostate segmentation algorithm has been tested by comparing its results with manual outlining and shown to have a mean error of −1.7% with a standard deviation of 3.1%.[277,278] Segmentation of the prostate requires about 8 s when implemented on a 2 GHz PC.

XV. SUMMARY

This subject area is clearly a large one to cover in a short review. The activity and contributions by the AAPM and medical physicists have not been at the same level as in imaging and treatment with ionizing radiation, where most medical physicists received their training. However, as illustrated, the contributions have been extensive in this major imaging and therapeutic modality.

[a]Electronic mail: pcarson@umich.edu

[1]L. V. Hefner and A. Goldstein, "Resonance by rod-shaped reflectors in ultrasound test objects," Radiology **139**, 189–193 (1981).
[2]W. T. Shi, F. Forsberg, J. S. Raichlen, L. Needleman, and B. B. Goldberg, "Pressure dependence of subharmonic signals from contrast microbubbles," Ultrasound Med. Biol. **25**(2), 275–283 (1999).
[3]M. C. Ziskin, A. Bonakdapour, D. P. Wienstein, and P. R. Lynch, "Contrast agents for diagnostic ultrasound," Invest. Radiol. **6**, 500–505 (1972).
[4]M. P. Andre, J. D. Craven, M. A. Greenfield, and R. Stern, "Measurement of the velocity of ultrasound in the human femur *in vivo*," Med. Phys. **7**(4), 324–330 (1980).
[5]F. J. Fry and L. K. Johnson, "Tumor irradiation with intense ultrasound," Ultrasound Med. Biol. **4**(4), 337–341 (1978).
[6]P. P. Lele, "Application of ultrasound in medicine," N. Engl. J. Med. **286**(24), 1317–1318 (1972).
[7]J. Tobias, K. Hynynen, and R. Roemer, "An ultrasound window to perform scanned, focused ultrasound hyperthermia treatments of brain tumors," Med. Phys. **14**(2), 228–234 (1987).
[8]M. Kinoshita, N. McDannold, F. A. Jolesz, and K. Hynynen, "Noninvasive localized delivery of Herceptin to the mouse brain by MRI-guided focused ultrasound-induced blood-brain barrier disruption," Proc. Natl. Acad. Sci. U.S.A. **103**(31), 11719–11723 (2006).
[9]N. McDannold and K. Hynynen, "Quality assurance and system stability of a clinical MRI-guided focused ultrasound system: Four-year experience," Med. Phys. **33**(11), 4307–4313 (2006).
[10]R. M. Arthur, W. L. Straube, J. D. Starman, and E. G. Moros, "Noninvasive temperature estimation based on the energy of backscattered ultrasound," Med. Phys. **30**(6), 1021–1029 (2003).
[11]A. B. Ross, C. J. Diederich, W. H. Nau, V. Rieke, R. K. Butts, G. Sommer, H. Gill, and D. M. Bouley, "Curvilinear transurethral ultrasound applicator for selective prostate thermal therapy," Med. Phys. **32**(6), 1555–1565 (2005).
[12]L. A. Crum and J. B. Fowlkes, "Acoustic Cavitation Generated by Microsecond Pulses of Ultrasound," Nature (London) **319**(6048), 52–54 (1986).
[13]D. L. Miller, W. L. Nyborg, and C. C. Whitcomb, "Platelet aggregation induced by ultrasound under specialized conditions *in vitro*," Science **205**(4405), 505–507 (1979).
[14]*Medical CT and Ultrasound: Current Technology and Applications*, AAPM Summer School Lectures (AAPM, College Park, MD, 1995).
[15]*Physics of Nonionizing Radiation* (Summer School Course Book). (AAPM, Boulder, CO, 1974).
[16]P. L. Carson and J. A. Zagzebski, "Pulse echo ultrasound imaging systems: Performance tests and criteria," AAPM Report #8 (1981), p. 73.
[17]M. M. Goodsitt, P. L. Carson, S. Witt, D. L. Hykes, and J. M. J. Kofler, "Real-time B-mode ultrasound quality control test procedures: Report of AAPM Ultrasound Task Group No. 1," Med. Phys. **25**(8), 1385–1406 (1998).
[18]T. S. Curry, J. E. Dowdey, and R. C. Murry, *Christensen's Physics of Diagnostic Radiology*, 4th ed. (Lea & Febiger, Philadelphia, 1992).
[19]W. R. Hedrick, D. L. Hykes, and D. E. Starchman, *Ultrasound Physics and Instrumentation* (Elsevier Mosby, St. Louis, 2004).
[20]W. R. Hendee and E. R. Ritenour, *Medical Imaging Physics* (Wiley-Liss, New York, 2002).
[21]D. H. Evans and W. N. McDicken, *Doppler Ultrasound: Physics, Instru-*

mentation (J. Wiley, New York, 2000).
[22]B. A. J. Angelsen, *Ultrasound Imaging: Waves, Signals, and Signal Processing* (Trondheim, Norway: Emantec AS, 2000).
[23]T. L. Szabo, *Diagnostic Ultrasound Imaging: Inside Out*. Academic Press Series in Biomedical Engineering, edited by J. Bronzino (Elsevier Academic Press, Burlington, 2004), p. 549.
[24]H. J. Smith and J. A. Zagzebski, *Basic Doppler Physics* (Medical Physics Publishing, Madison, WI, 1991).
[25]K. A. Griffiths, "An historical look at ultrasound as an Australian innovation on the occasion of the ultrasound stamp issued by Australia Post—18 May 2004," ASUM Ultrasound Bulletin **2004**(3), 22–26 (2004).
[26]D. Robinson, "Invent your own radiation," Presentation to sonographers in Australia, 1980's.
[27]D. Nicholas, "Evaluation of backscattering coefficients for excised human tissues: results, interpretation and associated measurements," Ultrasound Med. Biol. **8**, 17–28 (1982).
[28]K. K. Shung and G. A. Thieme, *Ultrasonic Scattering in Biological Tissues* (CRC Press, Boca Raton, FL, 1992).
[29]J. F. Greenleaf, *Tissue Characterization with Ultrasound* (CRC Press, Boca Raton, FL, 1986).
[30]F. Forsberg, B. B. Goldberg, Y. Wu, J. B. Liu, D. A. Merton, and N. M. Rawool, "Harmonic imaging with gas-filled microspheres: Initial experiences," Int. J. Imaging Syst. Technol. **8**(1), 69–81 (1997).
[31]K. Drukker, M. L. Giger, and E. B. Mendelson, "Computerized analysis of shadowing on breast ultrasound for improved lesion detection," Med. Phys. **30**(7), 1833–1842 (2003).
[32]J. M. Rubin, R. S. Adler, R. O. Bude, J. B. Fowlkes, and P. L. Carson, "Clean and dirty shadowing at US: A reappraisal," Radiology **181**(1), 231–236 (1991).
[33]X. Fan and K. Hynynen, "The effects of curved tissue layers on the power deposition patterns of therapeutic ultrasound beams," Med. Phys. **21**(1), 25–34 (1994).
[34]A. Moskalik, P. L. Carson, C. R. Meyer, J. B. Fowlkes, J. M. Rubin, and M. A. Roubidoux, "Registration of three-dimensional compound ultrasound scans of the breast for refraction and motion correction," Ultrasound Med. Biol. **21**(6), 769–778 (1995).
[35]A. Goldstein and B. L. Madrazo, "Slice-thickness artifacts in gray-scale ultrasound," J. Clin. Ultrasound **9**(7), 365–375 (1981).
[36]J. M. Rubin, R. S. Adler, J. B. Fowlkes, and P. L. Carson, "Phase cancellation: A cause of acoustical shadowing at the edges of curved surfaces in B-mode ultrasound images," Ultrasound Med. Biol. **17**(1), 85–95 (1991).
[37]T. R. Nelson, D. H. Pretorius, A. Hull, M. Riccabona, M. S. Sklansky, and G. James, "Sources and impact of artifacts on clinical three-dimensional ultrasound imaging," Ultrasound Obstet. Gynecol. **16**(4), 374–383 (2000).
[38]F. Forsberg, J. Liu, P. Burns, D. Merton, and B. Goldberg, "Artifacts ultrasound contrast agent studies," J. Ultrasound Med. **13**, 357–365 (1994).
[39]P. L. Carson and T. V. Oughton, "A modeled study for diagnosis of small anechoic masses with ultrasound," Radiology **122**, 765–771 (1977).
[40]D. Cathignol, O. A. Sapozhnikov, and J. Zhang, "Lamb waves in piezoelectric focused radiator as a reason for discrepancy between O'Neil's formula and experiment," J. Acoust. Soc. Am. **101**(3), 1286–1297 (1997).
[41]H. T. O'Neil, "Theory of focusing radiators," J. Acoust. Soc. Am. **21**(5), 516–526 (1949).
[42]P. Webb and C. Wykes, "Analysis of fast accurate low ambiguity beam forming for non lambda/2 ultrasonic arrays," Ultrasonics **39**(1), 69–78 (2001).
[43]T. A. Whittingham, "Transducers and beam forming in medical ultrasonic imaging," Insight **41**(1), 8–12 (1999).
[44]J. Y. Lu and J. Q. Cheng, "Field computation for two-dimensional array transducers with limited diffraction array beams," Ultrason. Imaging **27**(4), 237–255 (2005).
[45]P. D. Fox, J. Q. Chen, and J. Y. Lu, "Theory and experiment of Fourier-Bessel field calculation and tuning of a pulsed wave annular array," J. Acoust. Soc. Am. **113**(5), 2412–2423 (2003).
[46]G. McLaughlin, T.-L. Ji, and D. Napolitano, "Broad-beam imaging methods," Zonare Medical Systems, Inc., Mountain View, CA, 2007.
[47]G. McLaughlin and T.-L. Ji, "Broad-beam imaging," Zonare Medical Systems, Inc., 2004.
[48]L. Y. L. Mo, D. DeBusschere, D. Napolitano, A. Irish, S. Marschall, G. W. McLaughlin, Z. Yang, P. L. Carson, and J. B. Fowlkes, "Compact ultrasound scanner with built-in raw data acquisition capabilities," in *IEEE International Ultrasonic Symposium Preceedings* (IEEE, New York, 2007).
[49]R. Fisher, K. Thomenius, R. Wodnicki, R. Thomas, B. Khuri-Yakub, A. Ergun, and G. Yaralioglu, "Reconfigurable arrays for portable ultrasound," Proc.-IEEE Ultrason. Symp. **1–4**, 495–499 (2005).
[50]C. R. Hazard, R. A. Fisher, D. M. Mills, L. S. Smith, K. E. Thomenius, and R. G. Wodnicki, "Annular array beamforming for 2D arrays with reduced system channels," Proc.-IEEE Ultrason. Symp. **2–2**, 1859–1862 (2003).
[51]M. G. Maginness, J. D. Plummer, W. L. Beaver, and J. D. Meindl, "State of the art in two dimensional ultrasonic transducer array technology," Med. Phys. **3**(5), 312–318 (1976).
[52]J.-H. Mo, A. L. Robinson, D. W. Fitting, F. L. Terry, and P. L. Carson, "Micromachining for improvement of integrated ultrasonic transducer sensitivity," IEEE Trans. Electron Devices **37**(1), 134–140 (1990).
[53]C. Daft, P. Wagner, B. Bymaster, S. Panda, K. Patel, and I. Ladabaum. "CMUTs and electronics for 2D and 3D imaging: Monolithic integration, in-handle chip sets and system implications," Proc.-IEEE Ultrason. Symp. **1**, 463–474 (2005).
[54]R. Fisher, K. Thomenius, R. Wodnicki, R. Thomas, S. Cogan, C. Hazard, W. Lee, D. Mills, B. Khuri-Yakub, A. Ergun, and G. Yaralioglu, "Reconfigurable arrays for portable ultrasound," Proc.-IEEE Ultrason. Symp. **1**, 495–499 (2005).
[55]S. A. Goss, R. L. Johnston, and F. Dunn, "Comprehensive compilation of empirical ultrasonic properties of mammalian tissues," J. Acoust. Soc. Am. **64**(2), 423–457 (1978).
[56]S. A. Goss, R. L. Johnston, and F. Dunn, "Compilation of empirical ultrasonic properties of mammalian tissues. II," J. Acoust. Soc. Am. **68**(1), 93–108 (1980).
[57]F. Duck, *Physical Properties of Tissues* (Academic Press, London, 1990), p. 346.
[58]J. H. Holmes (Private communication, 1975).
[59]D. P. Shattuck, J. Ophir, G. W. Johnson, Y. Yazdi, and D. Mehta, "Correction of refraction and other angle errors in beam tracking speed of sound estimations using multiple tracking transducers," Ultrasound Med. Biol. **15**(7), 673–681 (1989).
[60]J. W. Mimbs, M. O'Donnell, and D. Bauwens, "The dependence of ultrasonic attenuation and backscatter on collagen content in dog and rabbit hearts," Circ. Res. **47**(1), 49–58 (1980).
[61]E. L. Madsen, G. R. Frank, P. L. Carson, P. D. Edmonds, L. A. Frizzell, B. A. Herman, F. W. Kremkau, W. D. O'Brien, K. J. Parker, and R. A. Robinson, "Interlaboratory comparison of ultrasonic attenuation and speed measurements," J. Ultrasound Med. **5**, 569–576 (1986).
[62]Z. F. Lu, J. A. Zagzebski, R. T. O'Brien, and H. Steinberg, "Ultrasound attenuation and backscatter in the liver during prednisone administration," Ultrasound Med. Biol. **23**(1), 1–8 (1997).
[63]R. Kuc and K. J. W. Taylor, "Variation of acoustic attenuation coefficient slope estimates for *in vivo* liver," Ultrasound Med. Biol. **8**(4), 403–412 (1982).
[64]M. F. Insana, "Modeling acoustic backscatter from kidney microstructure using an anisotropic correlation function," J. Acoust. Soc. Am. **97**, 649–655 (1995).
[65]C. R. Meyer, D. S. Herron, P. L. Carson, R. A. Banjavic, G. A. Thieme, F. L. Bookstein, and M. L. Johnson, "Estimation of ultrasonic attenuation and mean backscatterer size via digital signal processing," Ultrason. Imaging **6**(1), 13–23 (1984).
[66]D. Nicholas, "Evaluation of backscattering coefficients for excised human tissues: results, interpretation and associated measurements," Ultrasound Med. Biol. **8**, 17–28 (1982).
[67]J. P. Jones, "Current Problems in Ultrasonic Impediography," Natl. Bur. Stand. Spec. Publ. **453**, 253–258 (1975).
[68]M. Fatemi and J. F. Greenleaf, "Real-time assessment of the parameter of nonlinearity in tissue using 'nonlinear shadowing'," Ultrasound Med. Biol. **22**(9), 1215–1228 (1996).
[69]T. Sato, "Generalized ultrasonic percussion: imaging of ultrasonic nonlinear parameters and its medical and industrial applications," Jpn. J. Appl. Phys., Part 1 **33**(5 B), 2833–2836 (1994).
[70]W. K. Law, L. A. Frizzell, and F. Dunn, "Determination of the nonlinearity parameter B/A of biological media," Ultrasound Med. Biol. **11**(2), 307–318 (1985).
[71]Y. Zheng, S. Chen, W. Tan, R. Kinnick, and J. F. Greenleaf, "Detection of tissue harmonic motion induced by ultrasonic radiation force using pulse-

echo ultrasound and Kalman filter," IEEE Trans. Ultrason. Ferroelectr. Freq. Control **54**(2), 290–299 (2007).
[72]M. L. Palmeri, M. H. Wang, J. J. Dahl, K. D. Frinkley, and K. R. Nightingale, "Quantifying hepatic shear modulus *in vivo* using acoustic radiation force," Ultrasound Med. Biol. **34**(4), 546–558 (2008).
[73]J. Bercoff, M. Tanter, and M. Fink, "Supersonic shear imaging: A new technique for soft tissue elasticity mapping," IEEE Trans. Ultrason. Ferroelectr. Freq. Control **51**(4), 396–409 (2004).
[74]E. H. Chiang, R. S. Adler, C. H. Meyer, J. M. Rubin, D. K. Dedrick, and T. J. Laing, "Quantitative assessment of surface roughness using backscattered ultrasound: The effects of finite surface curvature," Ultrasound Med. Biol. **20**, 123–135 (1994).
[75]W. Liu, J. A. Zagzebski, T. Varghese, A. L. Gerig, and T. J. Hall, "Spectral and scatterer-size correlation during angular compounding: Simulations and experimental studies," Ultrason. Imaging **28**(4), 230–244 (2006).
[76]F. L. Lizzi, M. Ostromogilsky, E. J. Feleppa, M. C. Rorke, and M. M. Yaremko, "Relationship of ultrasonic spectral parameters to features of tissue microstructure," IEEE Trans. Ultrason. Ferroelectr. Freq. Control **UFFC-34**(3), 319–329 (1987).
[77]R. F. Wagner, S. W. Smith, J. M. Sandrik, and H. Lopez, "Statistics of speckle in ultrasound B-scans," IEEE Trans. Sonics Ultrason. **SU-30**(3), 156–163 (1983).
[78]T. Wilson, Q. Chen, J. A. Zagzebski, T. Varghese, and L. VanMiddlesworth, "Initial clinical experience imaging scatterer size and strain in thyroid nodules," J. Ultrasound Med. **25**(8), 1021–1029 (2006).
[79]K. K. Shung, G. Cloutier, and C. C. Lim, "The effects of hematocrit, shear rate, and turbulence on ultrasonic Doppler spectrum from blood," IEEE Trans. Biomed. Eng. **39**(5), 462–469 (1992).
[80]E. Bossy, M. Talmant, and P. Laugier, "Three-dimensional simulations of ultrasonic axial transmission velocity measurement on cortical bone models," J. Acoust. Soc. Am. **115**(5 I), 2314–2324 (2004).
[81]M. L. Oelze, W. D. O'Brien, Jr., J. P. Blue, and J. F. Zachary, "Differentiation and characterization of rat mammary fibroadenomas and 4T1 mouse carcinomas using quantitative ultrasound imaging," IEEE Trans. Med. Imaging **23**(6), 764–771 (2004).
[82]R. L. Nasoni, T. Bowen, M. W. Dewhirst, H. B. Roth, and R. Premovich, "Speed of sound as a thermal image CT scan parameter," in *Acoustical Imaging: Proceedings of the International Symposium*, Vol. 11, pp. 563–582 (Plenum Press, Monterey, CA, 1982).
[83]R. L. Nasoni, T. Bowen, W. G. Connor, and R. R. Sholes, "*In vivo* temperature dependence of ultrasound speed in tissue and its application to noninvasive temperature monitoring," Ultrason. Imaging **1**(1), 34–43 (1979).
[84]F. W. Kremkau, *Diagnostic Ultrasound: Principles and Instruments*. 7th ed. (W. B. Saunders Company, Philadelphia, 2006), p. 544.
[85]O. T. von Ramm, S. W. Smith, and H. E. Pavy, Jr., "High-speed ultrasound volumetric imaging system, Parallel processing and image display," IEEE Trans. Ultrason. Ferroelectr. Freq. Control **38**(2), 109–115 (1991).
[86]N. A. Baily, "A review of the processes by which ultrasound is generated through the interaction of ionizing radiation and irradiated materials: Some possible applications," Med. Phys. **19**(3), 525–532 (1992).
[87]T. Bowen, R. L. Nasoni, and A. E. Pifer, "Thermoacoustic Imaging Induced by deeply penetrating radiation," in *Acoustical Imaging: Proceedings of the International Symposium*, Vol. 13, pp. 409–427 (Plenum Press, Minneapolis, MN, 1984).
[88]A. A. Oraevsky, A. A. Karabutov, S. V. Solomatin, "Laser optoacoustic imaging of breast cancer *in vivo*," Proc. SPIE **4256**, 6–15 (2001).
[89]X. Wang, D. L. Chamberland, P. L. Carson, J. B. Fowlkes, R. O. Bude, D. A. Jamadar, and B. J. Roessler, "Imaging of joints with laser-based photoacoustic tomography: An animal study," Med. Phys. **33**(8), 2691–2697 (2006).
[90]Y. Wang, X. Xie, X. Wang, G. Ku, K. L. Bill, D. P. O'Neal, G. Stoica, and L. V. Wang, "Photoacoustic tomography of a nanoshell contrast agent in the *in vivo* rat brain," Nano Lett. **4**, 1689–1692 (2004).
[91]Q. Zhu, E. B. Cronin, A. A. Currier, H. S. Vine, M. Huang, N. Chen, and C. Xu, "Benign versus malignant breast masses: Optical differentiation with US-guided optical imaging reconstruction," Radiology **237**(1), 57–66 (2005).
[92]H. Jiang, C. Li, D. Pearlstone, and L. L. Fajardo, "Ultrasound-guided microwave imaging of breast cancer: Tissue phantom and pilot clinical experiments," Med. Phys. **32**(8), 2528–2535 (2005).
[93]H. F. Routh, "Doppler ultrasound," IEEE Eng. Med. Biol. Mag. **15**, 31–40 (1996).
[94]K. Ferrara and G. DeAngelis, "Color flow mapping," Ultrasound Med. Biol. **23**(3), 321–345 (1997).
[95]P. L. Carson, X. Li, J. Pallister, A. Moskalik, J. M. Rubin, and J. B. Fowlkes, "Approximate quantification of detected fractional blood volume and perfusion from 3D color flow and Doppler signal amplitude imaging.," *IEEE Ultrason. Symp. Proceeding*, pp. 1023–1026 (IEEE, Baltimore, 1993).
[96]J. M. Rubin, R. O. Bude, P. L. Carson, R. L. Bree, and R. S. Adler, "Power Doppler US: A potentially useful alternative to mean frequency-based color Doppler US," Radiology **190**(3), 853–856 (1994).
[97]P. A. Picot, D. W. Rickey, R. Mitchell, R. N. Rankin, and A. Fenster, "Three-dimensional colour doppler imaging," Ultrasound Med. Biol. **19**, 95–104 (1993).
[98]D. H. Pretorius, T. R. Nelson, and J. S. Jaffe, "3-dimensional sonographic analysis based on color flow Doppler and gray scale image data: A preliminary report," J. Ultrasound Med. **11**, 225–232 (1992).
[99]D. H. Pretorius, N. N. Borok, M. S. Coffler, and T. R. Nelson, "Three-dimensional ultrasound in obstetrics and gynecology," Radiol. Clin. North Am. **39**(3), 499–521 (2001).
[100]I. A. Hein, J. T. Chen, W. K. Jenkins, and W. D. O'Brien, Jr., "A real-time ultrasound time domain correlation blood flowmeter. I. Theory and design," IEEE Trans. Ultrason. Ferroelectr. Freq. Control **40**, 768–775 (1993a).
[101]F. W. Ferrara and V. R. Algazi, "A new wideband spread target maximum likelihood estimator for blood velocity estimation. Theory," IEEE Trans. Ultrason. Ferroelectr. Freq. Control **38**, 1–16 (1991a).
[102]P. Tortoli, G. Bambi, and S. Ricci, "Accurate Doppler angle estimation for vector flow measurements," IEEE Trans. Ultrason. Ferroelectr. Freq. Control **53**(8), 1425–1431 (2006).
[103]P. L. Carson, P. R. Fischella, and T. V. Oughton, "Ultrasonic power and intensities produced by diagnostic ultrasound equipment," Ultrasound Med. Biol. **3**, 341–350 (1978).
[104]E. L. Carstensen, W. K. Law, N. D. McKay, and T. G. Muir, "Demonstration of nonlinear acoustical effects at biomedical frequencies and intensities," Ultrasound Med. Biol. **6**(4), 359–368 (1980).
[105]F. A. Duck and H. C. Starritt, "Acoustic shock generation by ultrasonic imaging equipment," Br. J. Radiol. **57**(675), 231–240 (1984).
[106]B. Ward, A. C. Baker, and V. F. Humphrey, "Nonlinear propagation applied to the improvement of resolution in diagnostic medical ultrasound," J. Acoust. Soc. Am. **101**(1), 143–154 (1997).
[107]M. A. Averkiou, D. N. Roundhill, and J. E. Powers, "A new imaging technique based on the nonlinear properties of tissues," in Proc.-IEEE Ultrason. Symp. **1&2**, 1561–1566 (1997).
[108]D. R. Bacon and E. L. Carstensen, "Increased heating by diagnostic ultrasound due to nonlinear propagation," J. Acoust. Soc. Am. **88**(1), 26–34 (1990).
[109]P. L. Carson, editor, Special "Issue: Effects of nonlinear ultrasound propagation on output display indices," J. Ultrasound Med. **18**, 27–86 (1999).
[110]Y. Li and J. A. Zagnebski, "Computer model for harmonic ultrasound imaging," IEEE Trans. Ultrason. Ferroelectr. Freq. Control **47**(5), 1259–1272 (2000).
[111]P. N. Burns, D. Hope Simpson, and M. A. Averkiou, "Nonlinear imaging," Ultrasound Med. Biol. **26 Suppl 1**, S19–22 (2000).
[112]T. A. Krouskop, D. R. Dougherty, and F. S. Vinson, "A pulsed Doppler ultrasonic system for making non-invasive measurements of the mechanical properties of soft tissue," J. Rehabil. Res. Dev. **24**, 1–8 (1987).
[113]A. P. Sarvazyan, A. R. Skovoroda, S. Y. Emelianov, J. B. Fowlkes, J. G. Pipe, R. S. Adler, R. B. Buxton, and P. L. Carson, "Biophysical bases of elasticity imaging," in *Acoustical Imaging* (Plenum Press, New York, 1995), pp. 223–240.
[114]M. O'Donnell, A. R. Skovoroda, B. M. Shapo, and S. Y. Emelianov, "Internal displacement and strain imaging using ultrasound speckle tracking," IEEE Trans. Ultrason. Ferroelectr. Freq. Control **41**, 314–325 (1994).
[115]J. Ophir, I. Cespedes, H. Ponnekanti, Y. Yazdi, and X. Li, "Elastography: A quantitative method for imaging the elasticity of biological tissues," Ultrason. Imaging **13**, 111–134 (1991).
[116]J. B. Fowlkes, S. Y. Emelianov, J. G. Pipe, A. R. Skovoroda, P. L. Carson, R. S. Adler, and A. P. Sarvazyan, "Magnetic-resonance-imaging techniques for detection of elasticity variation," Med. Phys. **22**(11 Pt 1), 1771–1778 (1995).

[117]J. Ophir, I. Cespedes, B. Garra, H. Ponekanti, Y. Huang, and N. Maklad, "Elastography: Ultrasonic imaging of tissue strain and elastic modulus *in vivo*," Eur. J. Ultrasound **3**, 49–70 (1996).
[118]A. R. Skovoroda, S. Y. Emelianov, and M. O'Donnell, "Reconstruction of tissue elasticity based on ultrasound displacement and strain images," IEEE Trans. Ultrason. Ferroelectr. Freq. Control **42**, 747–765 (1995).
[119]A. Sarvazyan, O. Rudenko, S. Swanson, J. Fowlkes, and S. Emelianov, "Shear wave elasticity imaging: A new ultrasonic technology of medical diagnostics," Ultrasound Med. Biol. **24**(9), 1419–1435 (1998).
[120]D. L. Miller, G. J. R. Spooner, and A. R. Williams, "Photodisruptive laser nucleation of ultrasonic cavitation for biomedical applications," J. Biomed. Opt. **6**(3), 351–358 (2001).
[121]T. N. Erpelding, K. W. Hollman, and M. O'Donnell, "Bubble-based acoustic radiation force elasticity imaging," IEEE Trans. Ultrason. Ferroelectr. Freq. Control **52**(6), 971–979 (2005).
[122]S. Bharat, T. Varghese, E. L. Madsen, and J. A. Zagzebski, "Radio-frequency ablation electrode displacement elastography: A phantom study," Med. Phys. **35**(6), 2432–2442 (2008).
[123]M. Rao, Q. Chen, H. Shi, and T. Varghese, "Spatial-angular compounding for elastography using beam steering on linear array transducers," Med. Phys. **33**(3), 618–626 (2006).
[124]Lantheus Medical Imaging Updates Definity® Label To Modify Benefit/Risk Assessment Of The Product: FDA Approves Class Labeling Changes For Echo Contrast Agents 2008 [cited May 13]; Available from: http://www.lantheus.com/News.html
[125]K. Ferrara, R. Pollard, and M. Borden, "Ultrasound microbubble contrast agents: fundamentals and application to gene and drug delivery," Annu. Rev. Biomed. Eng. **9**, 415–447 (2007).
[126]M. Postema and G. Schmitz, "Bubble dynamics involved in ultrasonic imaging," Expert Rev. Mol. Diagn. **6**(3), 493–502 (2006).
[127]M. Andre, T. Nelson, and R. Mattrey, "Physical and acoustical properties of perfluorooctylbromide, an ultrasound contrast agent," Invest. Radiol. **25**(9), 983–987 (1990).
[128]R. M. Schmitt, H. J. Schmidt, and A. Irion, "Ultrasonic characterization of ultrasound contrast agents," in *Annual International Conference of the IEEE Engineering in Medicine and Biology Proceedings*, Vol. 11, pt 2, pp. 429–430 (Alliance for Engineering in Medicine and Biology, Seattle, 1989).
[129]D. L. Miller, "Ultrasonic detection of resonant cavitation bubbles in a flow tube by their second harmonic emissions," Ultrasonics **19**, 217–224 (1981).
[130]N. de Jong, "Acoustic properties of ultrasound contrast agents," Ph.D. thesis, Erasmus University (Rotterdam, 1993).
[131]P. N. Burns, J. E. Powers, and T. Fritzsch, "Harmonic imaging: New imaging and doppler method for contrast enhanced US," Radiology **185**, 142 (1992).
[132]P. N. Burns, J. E. Powers, D. Hope Simpson, V. Uhlendorf, and T. Fritzsch, "Harmonic imaging: Princples and preliminary results," Angiology **47**, S63–S74 (1996).
[133]T. R. Porter, F. Xie, D. Kricsfeld, and R. W. Armbruster, "Improved myocardial contrast with second harmonic transient ultrasound response imaging in humans using intravenous perfluorocarbon-exposed sonicated dextrose albumin," J. Am. Coll. Cardiol. **27**(6), 1497–1501 (1996).
[134]D. H. Simpson, C. T. Chin, and P. N. Burns, "Pulse inversion Doppler: A new method for detecting nonlinear echose from microbubble contrast agents," IEEE Trans. Ultrason. Ferroelectr. Freq. Control **46**(2), 372–382 (1999).
[135]T. Potdevin, J. Fowlkes, A. Moskalik, and P. Carson, "Analysis of refill curve shape in ultrasound contrast agent studies," Med. Phys. **31**(3), 623–632 (2004).
[136]N. G. Chen, J. B. Fowlkes, P. Carson, and G. L. LeCarpentier, "Rapid 3D imaging of contrast flow: Demonstration of a dual-beam technique," Ultrasound Med. Biol. **33**(6), 915–923 (2007).
[137]M. P. Andre, H. S. Janee, P. J. Martin, G. P. Otto, B. A. Spivey, and D. Palmer, "High-speed data acquisition in a diffraction tomography system employing large-scale toroidal arrays," Int. J. Imaging Syst. Technol. **8**, 137–147 (1997).
[138]P. L. Carson, C. R. Meyer, A. L. Scherzinger, and T. V. Oughton, "Breast imaging in coronal planes with simultaneous pulse echo and transmission ultrasound," Science **214**(4525), 1141–1143 (1981).
[139]T. R. Nelson, J. Nebeker, S. Denton, L. I. Cervino, D. H. Pretorius, and J. M. Boone, "Performance characterization of a volumetric breast ultrasound scanner," Progress in Biomedical Optics and Imaging, Proc. SPIE **6510**, P65101G (2007).
[140]J. A. Shipley, F. A. Duck, D. A. Goddard, M. R. Hillman, M. Halliwell, M. G. Jones, and B. T. Thomas, "Automated quantitative volumetric breast ultrasound data-acquisition system," Ultrasound Med. Biol. **31**(7), 905–917 (2005).
[141]S. L. Christensen and P. L. Carson, "Performance survey of ultrasound instrumentation and feasibility of routine monitoring," Radiology **122**, 449–454 (1977).
[142]M. L. Giger, H. Al-Hallaq, Z. Huo, C. Moran, D. E. Wolverton, C. W. Chan, and W. Zhong, "Computerized analysis of lesions in US images of the breast," Radiology **6**(11, Supp. 7), 665–674 (1999).
[143]B. Sahiner, H. P. Chan, M. A. Roubidoux, L. M. Hadjiiski, M. Helvie, C. Paramagul, J. Bailey, A. Nees, and C. Blane, "Malignant and benign breast masses on 3D US volumetric images: Effect of computer-aided diagnosis on radiologist accuracy," Radiology **242**, 716–724 (2007).
[144]P. T. Bhatti, G. L. LeCarpentier, M. A. Roubidoux, J. B. Fowlkes, M. A. Helvie, and P. L. Carson, "Discrimination of sonographically detected breast masses using frequency shift color Doppler imaging in combination with age and gray scale criteria," J. Ultrasound Med. **20**(4), 343–350 (2001).
[145]C. Sehgal, P. Arger, S. Rowling, E. Conant, C. Reynolds, and J. Patton, "Quantitative vascularity of breast masses by Doppler imaging: Regional variations and diagnostic implications," J. Ultrasound Med. **19**(7), 427–442 (2000).
[146]K. A. Dines, E. Kelly-Fry, and P. Romilly-Harper, "Automated three-dimensional ultrasound breast scanning in the craniocaudal mammography position," Ninth International Congress on the Ultrasonic Examination of the Breast, abstract booklet, pp. 43–44 (Indianapolis, IN, 1995).
[147]K. Richter, S. H. Heywang-Köbrunner, K. J. Winzer, K. J. Schmitt, H. Prihoda, H. D. Frohberg, H. Guski, P. Gregor, J. U. Blohmer, F. Fobbe, K. Döinghaus, G. Löhr, and B. Hamm, "Detection of malignant and benign breast lesions with an automated US system: Results in 120 cases," Radiology **205**(3), 823–830 (1997).
[148]S. P. Sinha, M. A. Roubidoux, M. A. Helvie, A. V. Nees, and M. M. Goodsitt, G. L. LeCarpentier, J. B. Fowlkes, C. L. Chaleck, and P. L. Carson, "Multi-modality 3D breast imaging with X-Ray tomosynthesis and automated ultrasound," 29th Annual International Conference IEEE Eng. Med. Biol. Soc., pp. 1335–1338 (Lyon, France, 2007).
[149]J. F. Greenleaf and R. C. Bahn, "Clinical imaging with transmissive ultrasonic computerized tomography," IEEE Trans. Biomed. Eng. **28**, 177–185 (1981).
[150]N. Duric, P. Littrup, A. Babkin, D. Chambers, S. Azevedo, A. Kalinin, R. Pevzner, M. Tokarev, E. Holsapple, O. Rama, and R. Duncan, "Development of ultrasound tomography for breast imaging: Technical assessment," Med. Phys. **32**(5), 1375–1386 (2005).
[151]R. M. Schmitt, C. R. Meyer, P. L. Carson, T. L. Chenevert, and P. H. Bland, "Error reduction in through transmission tomography using large receiving arrays with phase-insensitive signal processing," IEEE Trans. Sonics Ultrason. **31**(4), 251–258 (1984).
[152]P. L. Carson, T. V. Oughton, W. R. Hendee, and A. S. Ahuja, "Imaging soft tissue through bone with ultrasound transmission tomography by reconstruction," Med. Phys. **4**, 302–309 (1977).
[153]R. Koch, J. F. Whiting, D. C. Price, and J. F. McCaffrey, "Ultrasonic transmission tomography and pulse-echo imaging of the breast," Ultrason. Imaging **4**(2), 188–189 (1982).
[154]T. L. Chenevert, D. I. Bylski, P. L. Carson, C. R. Meyer, R. M. Schmitt, P. H. Bland, and D. Adler, "Ultrasonic computed tomography of the breast," Radiology **152**, 155–159 (1984).
[155]T. L. Chenevert, C. R. Meyer, P. H. Bland, and P. L. Carson, "Aperture diffraction theory applied to ultrasonic attenuation imaging," J. Acoust. Soc. Am. **74**(4), 1232–1238 (1983).
[156]C. R. Meyer, T. L. Chenevert, and P. L. Carson, "A method for reducing multipath artifacts in ultrasonic computed tomography," J. Acoust. Soc. Am. **72**(3), 820–823 (1982).
[157]P. L. Carson, A. L. Scherzinger, C. R. Meyer, W. Jobe, B. Samuels, and D. D. Adler, "Lesion detectability in ultrasonic computed tomography of symptomatic breast patients," Invest. Radiol. **3**, 421–427 (1988).
[158]A. L. Scherzinger, R. A. Belgam, P. L. Carson, C. R. Meyer, J. V. Sutherland, F. L. Bookstein, and T. M. Silver, "Assessment of ultrasonic computed tomography in symptomatic breast patients by discriminant analysis," Ultrasound Med. Biol. **15**, 21–28 (1989).
[159]N. Duric, P. Littrup, A. Babkin, D. Chambers, S. Azevedo, A. Kalinin, R. Pevzner, M. Tokarev, E. Holsapple, O. Rama, and R. Duncan, "Develop-

ment of ultrasound tomography for breast imaging: Technical assessment," Med. Phys. **32**(5), 1375–1386 (2005).
[160]F. Denis, O. Basset, and G. Gimenez, "Ultrasonic transmission tomography in refracting media-reduction of refraction artifacts by curved-ray techniques," IEEE Trans. Med. Imaging **14**(1), 173–188 (1995).
[161]A. Yamada and S. Yano, "Ultrasound inverse scattering computed tomography under the angular illumination limitation," Jpn. J. Appl. Phys., Part 1 **43**(8A), 5582–5588 (2004).
[162]N. Duric, A. Babkin, O. Rama, R. Pevzner, P. Littrup, L. Poulo, E. Holsapple, and C. Glide, "Detection of breast cancer with ultrasound tomography: First results with the Computed Ultrasound Risk Evaluation (CURE) prototype," Med. Phys. **34**(2), 773–785 (2007).
[163]K. S. Callahan, D. T. Borup, S. A. Johnson, J. Wiskin, and Y. Parisky, "Transmission breast ultrasound imaging: Representative case studies of speed of sound and attenuation of sound computed tomographic images," Am. J. Clin. Oncol. **30**(4), 458–459 (2007).
[164]E. Kelly-Fry and V. P. Jackson, "Adaptation development and expansion of x-ray mammography techniques for ultrasound mammography," J. Ultrasound Med. **10**, S–16 (1991).
[165]K. Richter, "Technique for detecting and evaluating breast lesions," J. Ultrasound Med. **13**, 797–802 (1994).
[166]P. L. Carson, A. P. Moskalik, A. Govil, M. A. Roubidoux, J. B. Fowlkes, D. Normolle, D. D. Adler, J. M. Rubin, and M. Helvie, "The 3D and 2D color flow display of breast masses," Ultrasound Med. Biol. **23**(6), 837–849 (1997).
[167]J. Suri, Y. Guo, C. Coad, T. Danielson, I. Elbakri, and R. Janer, "Image quality assessment via segmentation of breast lesion in x-ray and Ultrasound phantom images from Fischer's full field digital mammography and ultrasound (FFDMUS) system," Technol. Cancer Res. Treat. **4**(1), 83–92 (2005).
[168]R. Schmidt *et al.*, Preliminary experience with WhoBUS, an automated whole breast ultrasound scanner: Comparison with conventional handheld ultrasound, in Annual Meeting, Radiol. Soc. North America (Chicago, 2006).
[169]K. M. Kelly and L. K. Lourie, "SonoCine (R), a new method for ultrasound breast screening: Results in 500 high-risk patients," Radiology **221**(S Nov), 606 (2001).
[170]S. P. Sinha, M. M. Goodsitt, M. A. Roubidoux, R. C. Booi, G. L. LeCarpentier, C. R. Lashbrook, K. Thomenius, C. L. Chalek, and P. L. Carson, "Automated ultrasound scanning on a dual modality breast imaging system: Coverage and motion issues and solutions," J. Ultrasound Med. **26**(5), 645–655 (2007).
[171]K. A. e. a. Dines, "Computerized ultrasound tomography of the human head: Experimental results," Ultrason. Imaging **3**, 342–351 (1981).
[172]J. Ylitalo, J. Koivukangas, and J. Oksman, "Ultrasonic reflection mode computed tomography through a skull bone," IEEE Trans. Biomed. Eng. **37**(11), 1059–1066 (1990).
[173]K. Hynynen, "Focused ultrasound for blood-brain disruption and delivery of therapeutic molecules into the brain," Expert Opinion on Drug Delivery **4**(1), 27–35 (2007).
[174]F. J. e. a. Kirkham, "Transcranial measurement of blood velocities in the basal cerebral arteries using pulsed Doppler ultrasound: Velocity as an index of flow," Ultrasound Med. Biol. **12**(1), 15–21 (1986).
[175]F. J. Fry, "Transkull transmission of an intense focused ultrasonic beam," Ultrasound Med. Biol. **3**, 179–184 (1977).
[176]S. Behrens, K. Spengos, M. Daffertshofer, H. Schroeck, C. E. Dempfle, and M. Hennerici, "Transcranial ultrasound-improved thrombolysis: Diagnostic vs. therapeutic ultrasound," Ultrasound Med. Biol. **27**(12), 1683–1689 (2001).
[177]M. Pernot, J. F. Aubry, M. Tanter, J. L. Thomas, and M. Fink, "High power transcranial beam steering for ultrasonic brain therapy," Phys. Med. Biol. **48**(16), 2577–2589 (2003).
[178]J. Sun and K. Hynynen, "The potential of transskull ultrasound therapy and surgery using the maximum available skull surface area," J. Acoust. Soc. Am. **105**(4), 2519–2527 (1999).
[179]J. White, G. T. Clement, and K. Hynynen, "Transcranial ultrasound focus reconstruction with phase and amplitude correction," IEEE Trans. Ultrason. Ferroelectr. Freq. Control **52**(9), 1518–1522 (2005).
[180]S. W. Flax and M. O'Donnell, "Phase-aberration correction in medical ultrasound: Basic principles," IEEE Trans. Ultrason. Ferroelectr. Freq. Control **35**(6), 758–767 (1988).
[181]K. J. Haworth, J. B. Fowlkes, P. L. Carson, and O. D. Kripfgans, "Towards aberration correction of transcranial ultrasound using acoustic droplet vaporization," Ultrasound Med. Biol. **34**(3), 435–445 (2008).
[182]N. Quieffin, S. Catheline, R. K. Ing, and M. Fink, "Real-time focusing using an ultrasonic one channel time-reversal mirror coupled to a solid cavity," J. Acoust. Soc. Am. **115**(5 I), 1955–1960 (2004).
[183]S. C. Tang, G. T. Clement, and K. Hynynen, "A computer-controlled ultrasound pulser-receiver system for transskull fluid detection using a shear wave transmission technique," IEEE Trans. Ultrason. Ferroelectr. Freq. Control **54**(9), 1772–1783 (2007).
[184]K. Hynynen and F. A. Jolesz, "Demonstration of potential noninvasive ultrasound brain therapy through an intact skull," Ultrasound Med. Biol. **24**(2), 275–283 (1998).
[185]N. McDannold, N. Vykhodtseva, S. Raymond, F. A. Jolesz, and K. Hynynen, "MRI-guided targeted blood-brain barrier disruption with focused ultrasound: Histological findings in rabbits," Ultrasound Med. Biol. **31**(11), 1527–1537 (2005).
[186]K. Hynynen and G. Clement, "Clinical applications of focused ultrasound-the brain," Int. J. Hyperthermia **23**(2), 193–202 (2007).
[187]N. Vykhodtseva, N. McDannold, and K. Hynynen, "Induction of apoptosis *in vivo* in the rabbit brain with focused ultrasound and Optison," Ultrasound Med. Biol. **32**(12), 1923–1929 (2006).
[188]R. S. Balaban and V. A. Hampshire, "Challenges in small animal noninvasive imaging," ILAR J. **42**(3), 248–262 (2001).
[189]M. D. Sherar, M. B. Noss, and F. S. Foster, "Ultrasound backscatter microscopy images the internal structure of living tumour spheroids," Nature (London) **330**(6147), 493–495 (1987).
[190]D. E. Goertz, J. L. Yu, R. S. Kerbel, P. N. Burns, and F. S. Foster, "High-frequency Doppler ultrasound monitors the effects of antivascular therapy on tumor blood flow," Cancer Res. **62**(22), 6371–6375 (2002).
[191]D. E. Kruse, R. H. Silverman, R. J. Fornaris, D. J. Coleman, and K. W. Ferrara, "A swept-scanning mode for estimation of blood velocity in the microvasculature," IEEE Trans. Ultrason. Ferroelectr. Freq. Control **45**(6), 1437–1440 (1998).
[192]G. J. Czarnota, M. C. Kolios, J. Abraham, M. Portnoy, F. P. Ottensmeyer, J. W. Hunt, and M. D. Sherar, "Ultrasound imaging of apoptosis: high-resolution non-invasive monitoring of programmed cell death *in vitro*, *in situ* and *in vivo*," Br. J. Cancer **81**(3), 520–527 (1999).
[193]M. L. Oelze, W. D. O'Brien, Jr., J. P. Blue, and J. F. Zachary, "Differentiation and characterization of rat mammary fibroadenomas and 4T1 mouse carcinomas using quantitative ultrasound imaging," IEEE Trans. Med. Imaging **23**(6), 764–771 (2004).
[194]D. H. Turnbull, J. A. Ramsay, G. S. Shivji, T. S. Bloomfield, L. From, D. N. Sauder, and F. S. Foster, "Ultrasound backscatter microscope analysis of mouse melanoma progression," Ultrasound Med. Biol. **22**(7), 845–853 (1996).
[195]A. M. Cheung, A. S. Brown, L. A. Hastie, V. Cucevic, M. Roy, J. C. Lacefield, A. Fenster, and F. S. Foster, "Three-dimensional ultrasound biomicroscopy for xenograft growth analysis," Ultrasound Med. Biol. **31**(6), 865–870 (2005).
[196]K. C. Graham, L. A. Wirtzfeld, L. T. MacKenzie, C. O. Postenka, A. C. Groom, I. C. MacDonald, A. Fenster, J. C. Lacefield, and A. F. Chambers, "Three-dimensional high-frequency ultrasound imaging for longitudinal evaluation of liver metastases in preclinical models," Cancer Res. **65**(12), 5231–5237 (2005).
[197]L. A. Wirtzfeld, G. Wu, M. Bygrave, Y. Yamasaki, H. Sakai, M. Moussa, J. I. Izawa, D. B. Downey, N. M. Greenberg, A. Fenster, J. W. Xuan, and J. C. Lacefield, "A new three-dimensional ultrasound microimaging technology for preclinical studies using a transgenic prostate cancer mouse model," Cancer Res. **65**(14), 6337–6345 (2005).
[198]I. V. Huizen, G. Wu, M. Moussa, J. L. Chin, A. Fenster, J. C. Lacefield, H. Sakai, N. M. Greenberg, and J. W. Xuan, "Establishment of a serum tumor marker for preclinical trials of mouse prostate cancer models," Clin. Cancer Res. **11**(21), 7911–7919 (2005).
[199]A. Goldberg, P. Pakkiri, E. Dai, A. Lucas, and A. Fenster, "Measurements of aneurysm morphology determined by 3-d micro-ultrasound imaging as potential quantitative biomarkers in a mouse aneurysm model," Ultrasound Med. Biol. **33**(10), 1552–1560 (2007).
[200]L. M. Gan, J. Gronros, U. Hagg, J. Wikstrom, C. Theodoropoulos, P. Friberg, and R. Fritsche-Danielson, "Non-invasive real-time imaging of atherosclerosis in mice using ultrasound biomicroscopy," Atherosclerosis **190**(2), 313–320 (2007).
[201]J. W. Xuan, M. Bygrave, H. Jiang, F. Valiyeva, J. Dunmore-Buyze, D. W. Holdsworth, J. I. Izawa, G. Bauman, M. Moussa, S. F. Winter, N. M. Greenberg, J. L. Chin, M. Drangova, A. Fenster, and J. C. Lacefield,

"Functional neoangiogenesis imaging of genetically engineered mouse prostate cancer using three-dimensional power Doppler ultrasound," Cancer Res. **67**(6), 2830–2839 (2007).
[202]R. L. Maurice, M. Daronat, J. Ohayon, E. Stoyanova, F. S. Foster, and G. Cloutier, "Non-invasive high-frequency vascular ultrasound elastography," Phys. Med. Biol. **50**(7), 1611–1628 (2005).
[203]D. H. Turnbull, T. S. Bloomfield, H. S. Baldwin, F. S. Foster, and A. L. Joyner, "Ultrasound backscatter microscope analysis of early mouse embryonic brain development," Proc. Natl. Acad. Sci. U.S.A. **92**(6), 2239–2243 (1995).
[204]O. Aristizabal, D. A. Christopher, F. S. Foster, and D. H. Turnbull, "40-MHZ echocardiography scanner for cardiovascular assessment of mouse embryos," Ultrasound Med. Biol. **24**(9), 1407–1417 (1998).
[205]S. Srinivasan, H. S. Baldwin, O. Aristizabal, L. Kwee, M. Labow, M. Artman, and D. H. Turnbull, "Noninvasive, in utero imaging of mouse embryonic heart development with 40-MHz echocardiography," Circulation **98**(9), 912–918 (1998).
[206]B. K. McConnell, K. A. Jones, D. Fatkin, L. H. Arroyo, R. T. Lee, O. Aristizabal, D. H. Turnbull, D. Georgakopoulos, D. Kass, M. Bond, H. Niimura, F. J. Schoen, D. Conner, D. A. Fischman, C. E. Seidman, and J. G. Seidman, "Dilated cardiomyopathy in homozygous myosin-binding protein-C mutant mice," J. Clin. Invest. **104**(9), 1235–1244 (1999).
[207]C. Z. Behm and J. R. Lindner, "Cellular and molecular imaging with targeted contrast ultrasound," Ultrasound Q. **22**(1), 67–72 (2006).
[208]J. J. Rychak, J. Graba, A. M. Cheung, B. S. Mystry, J. R. Lindner, R. S. Kerbel, and F. S. Foster, "Microultrasound molecular imaging of vascular endothelial growth factor receptor 2 in a mouse model of tumor angiogenesis," Mol. Imaging **6**(5), 289–296 (2007).
[209]K. R. Erikson and P. L. Carson, "The AIUM standard 100 mm test object and recommended procedures for its use," Reflections **1–2**, 74–91 (1975).
[210]E. L. Madsen, J. A. Zagzebski, R. A. Banjavic, and R. E. Jutila, "Tissue mimicking materials for ultrasound phantoms," Med. Phys. **5**, 391–394 (1978).
[211]J. Ophir, "Ultrasound phantom material," Br. J. Radiol. **57**(684), 1161 (1984).
[212]J. Satrapa, G. Doblhoff, and H. J. Schultz, "Automated quality control of diagnostic ultrasound appliances," Ultraschall Med. **81**, 123–128 (2002).
[213]IEC, 60854 Methods of measuring the performance of ultrasonic pulse echo diagnostic equipment. 1986, Geneva: International Electrotechnical Commission.
[214]J. B. Fowlkes and C. K. Holland, "Mechanical bioeffects from diagnostic ultrasound: AIUM consensus statements," J. Ultrasound Med. **19**(2), 69–72 (2000).
[215]D. L. Miller, "A review of the ultrasonic bioeffects of microsonation, gas-body activation, and related cavitation-like phenomena," Ultrasound Med. Biol. **13**, 443–470 (1987).
[216]D. L. Miller, "WFUMB safety symposium on echo-contrast agents: *In vitro* bioeffects," Ultrasound Med. Biol. **33**, 197–204 (2007).
[217]J. B. Fowlkes, J. S. Abramowicz, C. C. Church, C. K. Holland, D. L. Miller, W. D. O'Brien Jr., N. T. Sanghvi, M. E. Stratmeyer, J. F. Zachary, C. X. Deng, G. R. Harris, B. A. Herman, K. H. Hynynen, C. R. B. Merritt, K. E. Thomenius, M. R. Bailey, P. L. Carson, E. L. Carstensen, L. A. Frizzell, W. L. Nyborg, S. B. Barnett, F. A. Duck, P. D. Edmonds, M. C. Ziskin, J. G. Abbott, D. Dalecki, F. Dunn, J. F. Greenleaf, K. A. Salvesen, T. A. Siddiqi, M. A. Averkiou, A. A. Brayman, E. C. Everbach, J. H. Wible, Jr., J. Wu, and D. G. Simpson, "AIUM consensus report on potential bioeffects of diagnostic ultrasound," J. Ultrasound Med. **27**(4), 515 (2008).
[218]AIUM/NEMA, Standard for Real-Time Display of Thermal and Mechanical Acoustic Output Indices on Diagnostic Ultrasound Equipment. Revision 2. AIUM/NEMA Standards Publication (NEMA UD3): Amer. Inst. Ultras. Med., Laurel, MD and Nat. Elect. Manuf. Assoc., Rosslyn, VA, 2004.
[219]NCRP-Comm-66, NCRP Report No. 140. Exposure criteria for medical diagnostic ultrasound: II. Criteria based on all known mechanisms: National Council on Radiation Protection and Measurements, Bethesda, 2002.
[220]T. A. Siddiqi, W. D. O'Brien, Jr., R. A. Meyer, J. M. Sullivan, and M. Miodovnik, "*In situ* human obstetrical ultrasound exposimetry: Estimates of derating factors for each of three different tissue models," Ultrasound Med. Biol. **21**(3), 379–391 (1995).
[221]C. C. Church and W. D. O'Brien, Jr., "Evaluation of the threshold for lung hemorrhage by diagnostic ultrasound and a proposed new safety index," Ultrasound Med. Biol. **33**(5), 810–818 (2007).
[222]D. L. Miller and J. Quddus, "Diagnostic ultrasound activation of contrast agent gas bodies induces capillary rupture in mice," Proc. Natl. Acad. Sci. U.S.A. **97**(18), 10179–10184 (2000).
[223]A. R. Williams, R. C. Wiggins, B. L. Wharram, M. Goyal, C. Dou, K. J. Johnson, and D. L. Miller, "Nephron injury induced by diagnostic ultrasound imaging at high mechanical index with gas body contrast agent," Ultrasound Med. Biol. **33**(8), 1336–1344 (2007).
[224]*IEEE Guide for Medical Ultrasound Field Parameter Measurements* (Institute of Electrical and Electronics Engineers, Inc., New York, 1990).
[225]C. Ziskin and P. A. Lewin, *Ultrasonic Exposimetry* (CRC Press, Boca Raton, FL, 1993).
[226]F. A. Duck and K. Martin, "Trends in diagnostic ultrasound exposure," Phys. Med. Biol. **36**, 1423–1432 (1991).
[227]FDA, 510(k) Guide for measuring and reporting output of diagnostic ultrasound medical devices, Center for Devices and Radiological Health, U.S. FDA, Rockville, MD (1995).
[228]IEC, 1157 Requirements for the declaration of the acoustic output of medical diagnostic ultrasound equipment (International Electrotechnical Commission Geneva, 1992).
[229]IEC, IEC 60601-2-37—Particular requirements for the safety of ultrasonic medical diagnostic and monitoring equipment, ed. 2 (I.E. Commission, Geneva, 2007).
[230]N. Grenier, H. Trillaud, J. Palussiere, C. Mougenot, B. Quesson, B. Denis De Senneville, and C. Moonen, "Therapies by focused ultrasound," Therapies par Ultrasons Focalises **88**(11 C2), 1787–1800 (2007).
[231]H. Wang, "Adaptive ultrasound phased array systems for deep hyperthermia," Ph.D. thesis, University of Michigan, 1994.
[232]NCRP, Exposure criteria for medical ultrasound. Part 1: Exposure based on thermal mechanisms. National Council on Radiation Protection and Measurements, Report 113 (National Council on Radiation Protection and Measurements, Bethesda, MD 1992).
[233]J. G. Lynn, R. L. Zwemer, A. J. Chick, and A. G. Miller, "A new method for the generation and use of focused ultrasound in experimental biology," J. Gen. Physiol. **26**, 179–193 (1942).
[234]A. K. Burov, "High-intensity ultrasonic vibrations for action on animal and human malignant tumours," Dokl. Akad. Nauk SSSR **106**, 239–241 (1956).
[235]R. C. Miller, W. G. Connor, R. S. Heusinkveld, and M. L. M. Boone, "Prospects for hyperthermia in human cancer therapy. I. Hyperthermic effects in man and spontaneous animal tumors," Radiology **123**(2), 489–495 (1977).
[236]A. Okada, T. Murakami, K. Mikami, H. Onishi, N. Tanigawa, T. Marukawa, and H. Nakamura, "A case of hepatocellular carcinoma treated by MR-guided focused ultrasound ablation with respiratory gating," Magn. Reson. Med. Sci. **5**(3), 167–171 (2006).
[237]S. Vaezy, X. Shi, R. W. Martin, E. Chi, P. I. Nelson, M. R. Bailey, and L. A. Crum, "Real-time visualization of high-intensity focused ultrasound treatment using ultrasound imaging," Ultrasound Med. Biol. **27**(1), 33–42 (2001).
[238]F. Wu, Z. B. Wang, W. Z. Chen, W. Wang, Y. Gui, M. Zhang, G. Zheng, Y. Zhou, G. Xu, M. Li, C. Zhang, H. Ye, and R. Feng, "Extracorporeal high intensity focused ultrasound ablation in the treatment of 1038 patients with solid carcinomas in China: An overview," Ultrason. Sonochem. **11**(3–4), 149–154 (2004).
[239]Z. Xu, T. L. Hall, J. B. Fowlkes, and C. A. Cain, "Effects of acoustic parameters on bubble cloud dynamics in ultrasound tissue erosion (histotripsy)," J. Acoust. Soc. Am. **122**(1), 229–236 (2007).
[240]J. E. Parsons, C. Cain, and G. D. Abrams, "Spatial variability in acoustic backscatter as an indicator of tissue homogenate production in pulsed cavitational ultrasound therapy," IEEE Trans. Ultrason. Ferroelectr. Freq. Control **54**, 576–590 (2007).
[241]M. D. Torno, M. D. Kaminski, Y. Xie, R. E. Meyers, C. J. Mertz, X. Liu, W. D. O'Brien, Jr., and A. J. Rosengart, "Improvement of *in vitro* thrombolysis employing magnetically-guided microspheres," Thromb. Res. **121**(6), 799–811 (2008).
[242]R. D. Zura, B. Sasser, V. Sabesan, R. Pietrobon, M. C. Tucker, and S. A. Olson, "A survey of orthopaedic traumatologists concerning the use of bone growth stimulators," J. Surg. Orthop. Advances **16**(1), 1–4 (2007).
[243]S. Vaezy and V. Zderic, "Hemorrhage control using high intensity focused ultrasound," Int. J. Hyperthermia **23**(2), 203–211 (2007).
[244]R. J. Siegal, S. Vaezy, R. Martin, and L. Crum, "High intensity focused ultrasound: A method of hemostasis," Echocardiogr. **18**(4), 309–315

(2001).
[245]P. L. Carson, W. W. Wenzel, P. Avery, and W. R. Hendee, "Ultrasound imaging as an aid to cancer therapy, Part II," Int. J. Radiat. Oncol., Biol., Phys. **1**, 335–343 (1976).
[246]M. A. Roubidoux, G. L. LeCarpentier, J. B. Fowlkes, B. Bartz, D. Pai, S. P. Gordon, A. F. Schott, T. D. Johnson, and P. L. Carson, "Sonographic evaluation of early-stage breast cancers that undergo neoadjuvant chemotherapy," J. Ultrasound Med. **24**, 885–895 (2005).
[247]D. J. Brewer, R. D. Dick, D. K. Grover, V. LeClaire, M. Tseng, M. Wicha, K. Pienta, B. G. Redman, T. Jahan, V. K. Sondak, M. Strawderman, G. L. LeCarpentier, and S. D. Merajver, "Treatment of metastatic cancer with tetrathiomolybdate, an anti-copper, antiangiogenic agent. I. Phase I. study," Clin. Cancer Res. **6**, 1–10 (2000).
[248]D. A. Kuban, L. Dong, R. Cheung, E. Strom, and R. De Crevoisier, "Ultrasound-based localization," Semin. Radiat. Oncol. **15**(3), 180–191 (2005).
[249]N. P. Orton, H. A. Jaradat, and W. A. Tome, "Clinical assessment of three-dimensional ultrasound prostate localization for external beam radiotherapy," Med. Phys. **33**(12), 4710–4717 (2006).
[250]K. Peignaux, G. Crehange, G. Truc, I. Barillot, S. Naudy, and P. Maingon, "High precision radiotherapy with ultrasonic imaging guidance," Cancer Radiother **10**(5), 231–234 (2006).
[251]F. Trichter and R. D. Ennis, "Prostate localization using transabdominal ultrasound imaging," Int. J. Radiat. Oncol., Biol., Phys. **56**(5), 1225–1233 (2003).
[252]W. A. Tome, S. L. Meeks, N. P. Orton, L. G. Bouchet, and F. J. Bova, "Commissioning and quality assurance of an optically guided three-dimensional ultrasound target localization system for radiotherapy," Med. Phys. **29**(8), 1781–1788 (2002).
[253]A. Hsu, N. R. Miller, P. M. Evans, J. C. Bamber, and S. Webb, "Feasibility of using ultrasound for real-time tracking during radiotherapy," Med. Phys. **32**(6), 1500–1512 (2005).
[254]J. Sylvester, J. C. Blasko, P. Grimm, and H. Ragde, "Interstitial implantation techniques in prostate cancer," J. Surg. Oncol. **66**(1), 65–75 (1997).
[255]D. Ash, D. M. Bottomley, and B. M. Carey, "Prostate brachytherapy," Prostate Cancer Prostatic Dis. **1**(4), 185–188 (1998).
[256]G. K. Edmundson, D. Yan, and A. A. Martinez, "Intraoperative optimization of needle placement and dwell times for conformal prostate brachytherapy," Int. J. Radiat. Oncol., Biol., Phys. **33**(5), 1257–1263 (1995).
[257]J. Pouliot, D. Tremblay, J. Roy, and S. Filice, "Optimization of permanent 125I prostate implants using fast simulated annealing," Int. J. Radiat. Oncol., Biol., Phys. **36**(3), 711–720 (1996).
[258]H. H. Holm and J. Gammelgaard, "Ultrasonically guided precise needle placement in the prostate and the seminal vesicles," J. Urol. **125**, 385–387 (1981).
[259]J. C. Blasko, K. Wallner, P. D. Grimm, and H. Ragde, "Prostate specific antigen based disease control following ultrasound guided 125iodine implantation for stage T1/T2 prostatic carcinoma," J. Urol. (Baltimore) **154**(3), 1096–1099 (1995).
[260]R. Nath, L. L. Anderson, G. Luxton, K. A. Weaver, J. F. Williamson, and A. S. Meigooni, "Dosimetry of interstitial brachytherapy sources: Recommendations of the AAPM Radiation Therapy Committee Task Group No. 43. American Association of Physicists in Medicine," Med. Phys. **22**(2), 209–234 (1995).
[261]M. Steggerda, C. Schneider, M. van Herk, L. Zijp, L. Moonen, and H. van der Poel, "The applicability of simultaneous TRUS-CT imaging for the evaluation of prostate seed implants," Med. Phys. **32**(7), 2262–2270 (2005).
[262]S. Tong, H. N. Cardinal, D. B. Downey, and A. Fenster, "Analysis of linear, area and volume distortion in 3D ultrasound imaging," Ultrasound Med. Biol. **24**(3), 355–373 (1998).
[263]Z. Wei, G. Wan, L. Gardi, G. Mills, D. Downey, and A. Fenster, "Robot-assisted 3D-TRUS guided prostate brachytherapy: System integration and validation," Med. Phys. **31**(3), 539–548 (2004).
[264]G. Fichtinger, E. C. Burdette, A. Tanacs, A. Patriciu, D. Mazilu, L. L. Whitcomb, and D. Stoianovici, "Robotically assisted prostate brachytherapy with transrectal ultrasound guidance—Phantom experiments," Brachytherapy **5**(1), 14–26 (2006).
[265]Z. Wei, L. Gardi, D. B. Downey, and A. Fenster, "Oblique needle segmentation and tracking for 3D TRUS guided prostate brachytherapy," Med. Phys. **32**(9), 2928–2941 (2005).
[266]G. Wan, Z. Wei, L. Gardi, D. B. Downey, and A. Fenster, "Brachytherapy needle deflection evaluation and correction," Med. Phys. **32**(4), 902–909 (2005).
[267]M. Ding, H. N. Cardinal, and A. Fenster, "Automatic needle segmentation in three-dimensional ultrasound images using two orthogonal two-dimensional image projections," Med. Phys. **30**(2), 222–234 (2003).
[268]M. Ding and A. Fenster, "A real-time biopsy needle segmentation technique using Hough transform," Med. Phys. **30**(8), 2222–2233 (2003).
[269]Z. Wei, L. Gardi, D. B. Downey, and A. Fenster, "Automated localization of implanted seeds in 3D TRUS images used for prostate brachytherapy," Med. Phys. **33**(7), 2404–2417 (2006).
[270]L. Phee, J. Yuen, D. Xiao, C. F. Chan, H. Ho, C. H. Thing, P. H. Tan, C. Cheng, and W. S. Ng, "Ultrasound guided robotic biopsy of the prostate," Int. J. Humanoid Robot. **3**(4), 463–483 (2006).
[271]A. Fenster, D. B. Downey, and H. N. Cardinal, "Three-dimensional ultrasound imaging," Phys. Med. Biol. **46**(5), R67–99 (2001).
[272]A. Fenster and D. B. Downey, "Three-dimensional ultrasound imaging and its use in quantifying organ and pathology volumes," Anal. Bioanal. Chem. **377**(6), 982–989 (2003).
[273]H. Bassan, T. Hayes, R. V. Patel, and M. Moallem, "A novel manipulator for 3D ultrasound guided percutaneous needle insertion," IEEE International Conference on Robotics and Automation Proceedings, pp. 617–622 (Rome, 2007).
[274]S. Tong, D. B. Downey, H. N. Cardinal, and A. Fenster, "A three-dimensional ultrasound prostate imaging system," Ultrasound Med. Biol. **22**(6), 735–746 (1996).
[275]F. Shao, "Efficient 3D prostate surface detection for ultrasound guided robotic biopsy," Int. J. Radiat. Oncol., Biol., Phys. **3**(4), 439–461 (2006).
[276]H. M. Ladak, Y. Wang, D. B. Downey, and A. Fenster, "Testing and optimization of a semiautomatic prostate boundary segmentation algorithm using virtual operators," Med. Phys. **30**(7), 1637–1647 (2003).
[277]Y. Wang, H. N. Cardinal, D. B. Downey, and A. Fenster, "Semiautomatic three-dimensional segmentation of the prostate using two-dimensional ultrasound images," Med. Phys. **30**(5), 887–897 (2003).
[278]M. Ding, B. Chiu, I. Gyacskov, X. Yuan, M. Drangova, D. B. Downey, and A. Fenster, "Fast prostate segmentation in 3D TRUS images based on continuity constraint using an autoregressive model," Med. Phys. **34**(11), 4109–4125 (2007).